Copyright Warning & Restrictions

The copyright law of the United States (Title 17, United States Code) governs the making of photocopies or other reproductions of copyrighted material.

Under certain conditions specified in the law, libraries and archives are authorized to furnish a photocopy or other reproduction. One of these specified conditions is that the photocopy or reproduction is not to be "used for any purpose other than private study, scholarship, or research." If a, user makes a request for, or later uses, a photocopy or reproduction for purposes in excess of "fair use" that user may be liable for copyright infringement,

This institution reserves the right to refuse to accept a copying order if, in its judgment, fulfillment of the order would involve violation of copyright law.

Please Note: The author retains the copyright while the New Jersey Institute of Technology reserves the right to distribute this thesis or dissertation

Printing note: If you do not wish to print this page, then select "Pages from: first page # to: last page #" on the print dialog screen

ABSTRACT

COMPOUND FLOODING IN COASTAL AREAS EMANATING FROM INLAND AND OFFSHORE EVENTS

by
Hamed Behzad Koochaksaraii

The vulnerability of urban populations to natural hazards and climate change is a major theme in many reports on coastal cities with flooding ranking highly among the climate change concerns. Flooding could occur as a result of runoff for inland rainfall that accumulates at the mouth of the estuary to the sea or it could occur due to a storm surge emanating from the ocean. The techniques for modeling the flooding from these events are very different, as they were developed in different scientific fields: hydrology and hydraulic engineering for inland rainfall versus coastal oceanography and coastal engineering for offshore storms. Therefore, there is no framework to combine the two approaches. Many studies have been conducted to show that there is a high probability of co-occurrence for these two events which is so-called *compound flooding*. Therefore, this research sought to provide a holistic framework that combines the two approaches.

The township of Old Bridge, New Jersey has been chosen as the study domain for this investigation. For flooding due to inland rainfall, SWMM (Storm Water Management Model) Software developed by the EPA has been used to provide the discharge to input to the model HEC-RAS (developed by U.S. Army Corps of Engineers). ArcGIS also used to extract the bathymetry profiles of the study domain and to define the land use properties, as those impact runoff speed and infiltration. Results for 100-year return period precipitation show more than a 3 ft of water level rise in the river which caused flooding in low areas. For offshore storms, data from Hurricane Sandy, extracted from the NOAA

website, has been used for simulating the 100-year ocean storm. The two-dimensional analysis conducted using the CHAMP software, developed by the U.S. Army, to determine the storm surge, wave height in flooded lands, and wave run-up elevation. These were used to delineate the flooded zones according to FEMA specifications (AE and VE) based on the Sea Water Elevation (SWEL) and wave heights.

Finally, MIKE-21 software has been used to model the compound flooding in the study domain. The results from the MIKE-21 show that the inundation depth increases significantly during the compound flooding. Also, by applying a certain river flow rates on the different storm surges, it can be concluded that the water level rise due to rainfall has a reverse relationship with mean sea level elevation. It means as the storm surge increases in the coastal area, the effect of flooding caused by rainfall decreases.

COMPOUND FLOODING IN COASTAL AREAS EMANATING FROM INLAND AND OFFSHORE EVENTS

by

Hamed Behzad Koochaksaraii

A Dissertation
Submitted to the Faculty of
New Jersey Institute of Technology
in Partial Fulfillment of the Requirements for the Degree of
Doctor of Philosophy in Environmental Engineering

John A. Reif, Jr. Department of Civil and Environmental Engineering

May 2020

APPROVAL PAGE

COMPOUND FLOODING IN COASTAL AREAS EMANATING FROM INLAND AND OFFSHORE EVENTS

Hamed Behzad Koochaksaraii

Dr. Michel Boufadel, Dissertation Advisor Professor of Civil and Environmental Engineering, NJIT	Date
Dr. Taha Marhaba, Committee Member Professor of Civil and Environmental Engineering, NJIT	Date
Dr. Fadi Karaa, Committee Member Associate Professor of Civil and Environmental Engineering, NJIT	Date
Dr. Bruno Gonsalves Da Silva, Committee Member Assistant Professor of Civil and Environmental Engineering, NJIT	Date
Dr. Zeyuan Qiu, Committee Member Professor of Chemistry and Environmental Science, NJIT	Date

BIOGRAPHICAL SKETCH

Author: Hamed Behzad Koochaksaraii

Degree: Doctor of Philosophy

Date: May 2020

Undergraduate and Graduate Education:

- Doctor of Philosophy in Environmental Engineering,
  New Jersey Institute of Technology, Newark, NJ, 2020

- Master of Marine Structure,
  Tarbiat Modares University, Tehran, Iran, 2016

- Bachelor of Science in Civil Engineering,
  University of Tehran, Tehran, Iran, 2013

Major: Environmental Engineering

Presentations and Publications:

Behzad, H., Boufadel, M., Tracking of *Water Level Rise During a Compound Flooding*, 2020. (In preparation).

Behzad, H., Cui, F., Boufadel, M., *Efficiency of Countermeasures on Protection the Shoreline of Bays with Narrow Inlet*, 2020. (In preparation)

Cui, F., Behzad, H., Zhao, L., Boufadel, M., *On the Dispersion of Oil Droplets in Rivers*, Journal of Hydraulic Engineering, 2020. (In review)

Behzad, H., Sanaei, P., *On Optimizing the Wave Energy Converters Configuration in a Farm*, Flood Mechanics Research Journal, 2019.

Behzad, H, Effect of Barrier Islands on Flood Mitigation in Barnegat Bay, New Jersey Association for Floodplain Management Conference, 2018.

Behzad, H., Panahi, R., *Optimization of Bottom-Hinged Flap-Type Wave Energy Converter for a Specific Wave-Rose*, Marine Science and Application Journal, 2017.

To my friends and family who saved me on rainy days, when the dark feels endless.

TABLE OF CONTENTS

Chapter **Page**

1 INTRODUCTION 1

2 BACKGROUND 5

3 METHODS 11

3.1 SWMM Software 11

3.1.1 Governing Equation 13

3.1.2 Routing Method 15

3.2 HEC-RAS: 16

3.3 CHAMP: 18

3.3.1 Flood Map Zones 18

3.3.2 WHAFIS Module 19

3.3.3 Run-up Module 24

3.4 MIKE-21 28

3.4.1 Wave-Wind Theory 30

3.5 Compound Flooding 31

4 RESEARCH ALGORITHM 34

4.1 Precipitation Analysis 34

4.1.1 Routing Method 37

4.1.2 Manning's Constant 38

4.1.3 Infiltration and Depression Storage 38

4.2 Inland Flooding 38

4.3 Ocean Flooding 42
4.3.1 Vegetation Effect 44
4.4 Compound Flooding 45
5 RESULTS 48
5.1 SWMM 48
5.2 HEC-RAS 51
5.2.1 Levees 56
5.2.2 Backwater of the Bridge 58
5.3 CHAMP 63
5.4 MIKE-21 67
5.4.1 Flow in the River 67
5.4.2 Ocean Storm Surge 68
6 SUMMARY & CONCLUSION 74
7 REFERENCES 78

CHAPTER 1

INTRODUCTION

The vulnerability of urban populations to natural hazards and climate change is a major theme in many reports on coastal cities with flooding ranking highly among the climate change concerns ((Jean-Baptiste, Kabisch, and Kuhlicke 2013). Based on National Oceanic and Atmospheric Administration (NOAA), counties in the US directly on the shoreline constitute less than 10 percent of the total land area but account for 39 percent of the total population. From 1970 to 2010, the population of these counties increased by almost 40% to reach 125 million in 2010 and is projected to increase by an additional 10 million people or 8% by 2020. In fact, the population density of coastal shoreline counties is over six times greater than the corresponding inland counties (NOAA 2013). And unfortunately, the coastal areas are vulnerable to both extreme storms from inland precipitation and ocean storms.

These coastal areas are experiencing huge storms every year that cause a tremendous amount of damage to the resident's properties. Hurricane Sandy in 2012 was one of the biggest storms ever happened on the US east coast (C. Kemp and Horton 2013) and (Hughes et al. 2014). Tide gages located at Raritan Bay, New Jersey show that maximum still water elevation (SWEL) reaching almost 10 ft above the mean sea level (NOAA). A maximum wave height of 32 ft has been recorded at the same gages. The total death toll reached 285, including at least 125 deaths in the United States., and more than 600,000 housing units were destroyed in New Jersey and New York. The government of New York City estimates that $19 billion in damage was inflicted on the city alone. Over 8 million people lost power during the event, and outages were seen for days in some major

cities, while outlying areas were without power for weeks. Power outages from Sandy were experienced as far west as Michigan. The hurricane caused over $70 billion in damage in the United States and was thus the fourth most expensive storm in U.S. history.

Due to the effect of sea-level rise, the return period of Hurricane Sandy's flood height decreased by a factor of ∼3× from the year 1800 to 2000 and is estimated to decrease by a further ∼5× from 2000 to 2100 under a moderate-emissions pathway. That means the return period of a storm the same size as Hurricane Sandy can be decreased from 300 years to 20 years in 2100 (Lin et al. 2016).

Based on the reports of the damages from Hurricane Sandy and other hurricanes in recent years, and the risk of more extreme storms in the future, protecting the coastal areas is a huge concern for the US, which spends large sums of money to mitigate flooding.

Flooding in coastal areas developed by extreme rainfalls is more frequent than the huge hurricanes, and they can cause other types of misfunction in residential areas. The impact of these types of rainfalls can be changed by modifications to land cover and to stream and river channels. In urban areas, such modifications are at their most extreme on their effects on human lives. In particular, there is much to suggest that many forms of adaptation to reduce the impacts of flooding, especially increasing building resilience, widening drainage channels, and creating detention ponds, which are extremely difficult to achieve in low-income settlements. (Douglas 2018).

Finally, studies showed that the co-occurrence of storm surge and rainfall event can magnify the amplitude of each other, and extreme water levels resulting from a combination of storm-tide flooding and riverine flooding are also known as compound flood events (Kumbier et al. 2018). The joint-probability analysis highlighted significant

dependence between extreme rainfall and extreme storm surges (Svensson and Jones 2006) and (Zheng et al. 2014).

There are different types of mechanisms that are most likely to happen during the compound flooding:

1) The joint occurrence of both may elevate water levels to a point where flooding is initiated, or its impacts exacerbated.

2) Destructive storm surge already causes widespread flooding, such that any significant rainfall on top of this (even if it is not an extreme event on its own) increases the flood depth and/or extent of the inundated area.

3) During a moderate storm surge that does not directly cause flooding but is high enough to fully block or slow down gravity-fed stormwater drainage, such that precipitation is more likely to cause flooding.

Some of these mechanisms are applicable to our study domain which will be discussing widely in upcoming chapters.

The main goal of this study is not to study the probability of compound flooding, but to investigate the magnitude and effect of the flooding in these coastal areas which are vulnerable to either extreme rainfalls, ocean storms or a combination of both.

The township of Old Bridge, New Jersey has been chosen as the study domain to simulate the 100-years return period inland and offshore storms. For flooding due to inland rainfall, the Storm Water Management Model (SWMM) software, developed by the EPA and HEC-RAS (developed by U.S. Army Corps of Engineers) were used. ArcGIS was also used for watershed delineation, define the land use properties and extract the bathymetry profiles of the study domain. SWMM software has been used to assign hydrodynamic and geological parameters to sub-sections of the study domain, simulate the precipitation and derive the flow hydrograph in the rivers. Afterward, the derived flow hydrograph was used as the input of HEC-RAS software to calculate the water level rise in the river. For offshore

storms, data from Hurricane Sandy, extracted from the NOAA website, has been used for simulating the 100-year ocean storm. The two-dimensional analysis was conducted using the CHAMP software, developed by U.S. Army, to determine the storm surge, wave height in flooded lands, wave run-up elevation and labeling the flooded zones (AE and VE) based on the Sea Water Elevation (SWEL) and wave heights. Finally, The MIKE-21 software has been used to simulate the compound flooding in the study domain. MIKE-21 uses the depth-averaged method to solve the flow domain which is a fast method on large scale computations. This ability makes it a suitable tool for the goals of this study.

CHAPTER 2

BACKGROUND

The Emergency Events Database (EM-DAT) from the Université Catholique de Louvain indicated that floods accounted for 40% of disasters in 2015, affecting more than 27 million people and causing more than $21 billion in losses. Therefore, mitigating the impacts of unavoidable natural disasters is necessary for efficient land utilization and sustainable economic growth (Sado-Inamura and Fukushi 2019).

(Noori et al. 2016) have explored the linkage between historical, current and future land use/land cover (LULC) conditions and peak flow and runoff volumes in a coastal community in Alabama to identify critical areas for downstream flooding. HEC-HMS hydrologic model used to study the flood risk. The model showed a significant increase in peak flow and runoff volume from 1966 to 2011 and from 2011 to 2022 due to urbanization. The sensitivity of peak flows to LULC change decreased with increasing storm return periods. They also showed that the increase was more significant for peak flow than for runoff volume. The results of this study clearly showed that even if there is the same level of urbanization at different parts of a watershed, their contribution to peak flow at a downstream point depends on their locations within the watershed.

(Woodruff, Irish, and Camargo 2013) used Accumulated Cyclone Energy (ACE) as a common metric parameter to comparing the overall tropical cyclone activity of different tropical cyclone regions; it is calculated by taking the sum of each tropical cyclone's maximum wind speed squared for all storms passing through a selected area. Storm surge is also related to wind speed squared thus ACE is a useful measure of both tropical cyclone activity and tropical cyclone surge potential.

(Pardue et al. 2005) conducted research to provide an initial assessment of contaminants present in floodwaters shortly after the storm and to characterize water pumped out of the city into Lake Pontchartrain once dewatering operations began several days after the storm. Data are presented which demonstrate that during the weeks following the storm, floodwater was brackish and well-buffered with very low concentrations of volatile organic pollutants.

(Ng and Mendelsohn 2005) have calculated the potential economic costs of sea-level rise for Singapore. The cost of protection and the cost of inundation are compared. Cost-benefit analysis shows that protection is the most desirable and efficient solution to sea-level rise for the market land of Singapore. Even if construction and maintenance costs are higher than expected, the total protection cost is still significantly lower than the benefit. Sea walls must be built along an entire coast to be effective. This result may not be applied universally around the world. Sites with much lower land values may have to be inundated as the cost of protection may exceed the land value.

(Shepard, Crain, and Beck 2011) found that salt marsh vegetation had a significant positive effect on wave attenuation as measured by reductions in wave height per unit distance across marsh vegetation. Saltmarsh vegetation also had a significant positive effect on shoreline stabilization as measured by accretion, lateral erosion reduction, and marsh surface elevation change. Saltmarsh characteristics that were positively correlated to both wave attenuation and shoreline stabilization were vegetation density, biomass production, and marsh size.

(Wang et al. 2014) Describes the application of a modeling system consisting of large-scale storm tide and a high-resolution inundation model for New York City during

Hurricane Sandy. They used a large-scale, unstructured grid storm tide model, semi-implicit Eulerian-Lagrangian Finite Element (SELFE), to hindcast water level variation during Hurricane Sandy in the mid-Atlantic portion of the U.S. East Coast. The results from large-scale model used as a boundary condition of the inundation model of NYC. For the inundation modeling, the sub-grid modeling technique in UnTRIM was used, which incorporates high-resolution LIDAR data of land heights and water depths in the sub-element of the computational grid. It provides more accurate calculations of conveyance fluxes, wetting and drying areas, and the bottom stress without having to make computations on the fine computation mesh, and so achieves savings of computational cost

(Wang and Christensen 1987) introduced the friction factor for a different type of land use (residential, forest, grass, etc.) for hurricane-induced surges. They presented an empirical friction factor based on water depth, drag coefficient and disposition parameter (obstacle diameter divided by the distance between obstacles). They showed that the drag coefficient has a tendency to become constant and equal to 1.0 when the disposition parameter is larger than 10.

(Smallegan et al. 2016) have used the numerical model XBeach to evaluate the morphological response of a developed barrier island fronted with a buried seawall response of Bay Head, NJ during Hurricane Sandy (2012). From their results, the seawall in Bay Head clearly served to protect coastal infrastructure and preserve the dune system during and after the storm. XBeach simulations indicate morphological change during two phases. In Phase 1, wave attack and ocean surge reach maximum values, and the seawall reduces wave forces by a factor of 1.7. In the absence of the seawall, dune heights are lowered, making the island vulnerable to wave action and flooding. During Phase 2, wave

attack is small, but bay water levels increase rapidly over 2 m within 6 h after Hurricane Sandy's landfall, exceeding ocean water levels. Although this bay-side flooding caused catastrophic erosion in the absence of the seawall (an additional 5 m of sediment eroded), no significant additional erosion is observed in the “seawall” case since the dune system remained intact.

(Orton et al. 2015) demonstrate that reductions in the depth of inlets or estuary channels can be used to reduce or prevent coastal flooding. Stevens ECOM hydrodynamic model (SECOM) of Jamaica Bay, New York is used to testing nature-based adaptation measures in ameliorating flooding for NYC’s two largest historical coastal flood events. They used two scenarios of shallowing all areas deeper than 2 m in the bay to be 2 m below Mean Low Water and shallowing only the narrowest part of the inlet to the bay. They result in peak water level reductions of 15%, and 6.8% for Hurricane Sandy, and 46% and 30% for the Category-3 hurricane, respectively.

(Wei et al. 2015) have studied the dynamic impact of a strong tsunami bore on several simplified bridge piers by an SPH model. This study shows that high bed shear stress zones caused by the tsunami bore are extended downstream of the bridge pier, where the accumulated potential energy is transformed into the kinetic energy due to a sudden flow expansion. To move a sediment particle that is initially at rest on a surface, the bed shear stress τ_b exerted by the fluid must exceed the critical shear stress τ_c of the sediment particle. Bed shear stress can be estimated by square of water velocity. They showed that there are two factors that cause a force on the piers; One is the total drag force on the pier, which is related to the size and the shape of the pier. The other is the force due to the blockage effect by the bridge pier, which is a function of the dimensionless cross-section

width of the pier (D/W). Finally, their results show that the circular pier has the least forces and the diamond pier has the highest.

(Ward et al. 2018) carried out research to analyzing the statistical dependence between observed sea-levels and river discharge for 187 combinations of stations across the globe. Dependence was assessed using *Kendall's rank correlation coefficient* (τ) and *copula models*. They found significant dependence for storm surge conditional on annual maximum discharge at 22% of the stations studied, and for discharge conditional on annual maximum storm surge at 36% of the stations studied. Allowing a time-lag between the two variables up to 5 days, the dependence for storm surge conditional on annual maximum discharge at 56% of stations, and for discharge conditional on annual maximum storm surge at 54% of stations.

(Hendry et al. 2019) used the *dependence method* with Kendall rank correlation and *joint-occurrence method* to assess the potential compound flooding in UK coastal areas. They found that in some areas the storms that generate high skew surges and high river discharge are typically similar in characteristics (western UK coastline for their case). In contrast, in some areas, the storms that typically generate high skew surges are mostly distinct from the types of storms that tend to generate high river discharge (eastern UK coastline for their case).

Also, they found that the high skew surges tend to occur more frequently with high river discharge at catchments with a lower base flow index, smaller catchment area, and steeper elevation gradient. In catchments with a high base flow index, large catchment area, and shallow elevation gradient, the peak river flow tends to occur several days after the high skew surge.

(Wahl et al. 2015) has used the MATLAB T_Tide package for a year-by-year harmonic tidal analysis to investigate the chance of compound flooding in the US coastline. They found that the risk of compound flooding is higher for the Atlantic/Gulf coast relative to the Pacific coast. Also, they have introduced three different mechanisms that can happen during the compound flood which cause more extreme conditions in coastal areas.

CHAPTER 3

METHODS

3.1 SWMM Software

SWMM conceptualizes a sub-catchment as a rectangular surface that has a uniform slope S and a width W that drains to a single outlet channel as shown in Figure 3.1. Overland flow is generated by modeling the sub-catchment as a nonlinear reservoir, as sketched in Figure 3.2.

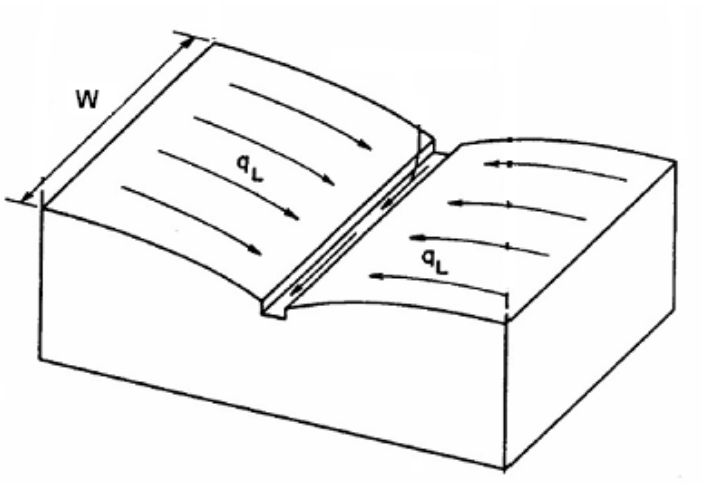

Figure 0.1 Idealized representation of a sub-catchment.

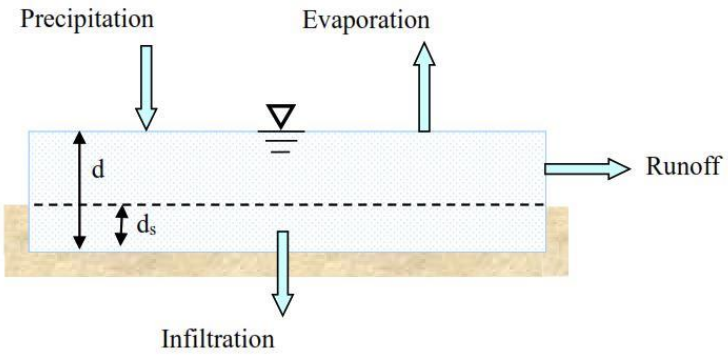

Figure 3.2 Nonlinear reservoir model of a sub-catchment.

If the sub-catchment has the appearance of Figure 3.1, then the width is approximating twice the length of the main drainage channel through the catchment. However, if the drainage channel is on the side of the catchment, the width is just the length of the channel. A good estimate for the width can be obtained by determining the average maximum length of overland flow and dividing the area by this length.

Most real sub-catchments will be irregular in shape and have a drainage channel that is off-center, as in Figure 3.3. This is especially true of rural or undeveloped catchments. A simple way of handling this case is given by (DiGiano, Adrian, and Mangarella 1977). A skew factor may be computed:

$$Z = A_m / A \tag{3.1}$$

Where Z is the skew factor, $0.5 \le Z \le 1$, A_m is the larger of the two areas on each side of the channel and A is the total area.

If L is the length of the main drainage channel, then the width W is simply a weighted sum between the two limits of L and $2L$:

$$W = L + 2L(1 - Z) \tag{3.2}$$

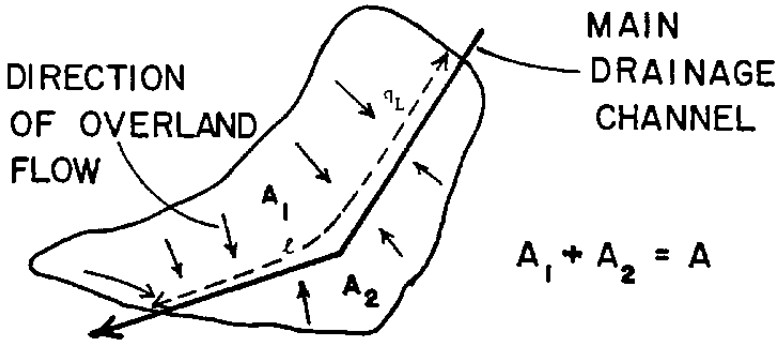

Figure 3.3 Irregular sub-catchment shape for width calculations.

The sub-catchment experiences inflow from precipitation (rainfall and snowmelt) and losses from evaporation and infiltration. The net excess ponds atop the sub-catchment surface to depth d. Ponded water above the depression storage depth d_s can become runoff outflow q. Depression storage accounts for initial rainfall abstractions such as surface ponding, an interception by flat roofs and vegetation, and surface wetting.

3.1.1 Governing Equation

From the conservation of mass, the net change in depth d per unit of time t is simply the difference between inflow and outflow rates over the sub-catchment:

$$\frac{\partial d}{\partial t} = i - e - f - q \tag{3.3}$$

where i is the rate of rainfall + snowmelt (ft/s), e is the surface evaporation rate (ft/s), f is the infiltration rate (ft/s) and q is the runoff rate (ft/s).

Note that the fluxes i, e, f, and q are expressed as flow rates per unit area $(cfs/ft^2 = ft/s)$.

Assuming that flow across the sub-catchment's surface behaves as if it were uniform flow within a rectangular channel of width W (ft), height d, and slope S, the Manning equation can be used to express the runoff's volumetric flow rate Q (cfs) as:

$$Q = \frac{1.49}{n} S^{0.5} R_x^{2/3} A_x \tag{3.4}$$

Here n is a surface roughness coefficient, S the apparent or average slope of the sub-catchment (ft/ft), A_x the area across the sub-catchment's width through which the runoff flows (ft^2), and R_x is the hydraulic radius associated with this area (ft). Referring to Figure 1 and Figure 3.2, A_x is a rectangular area with width W and height d. Because W will always be much larger than d it follows that $A_x = W(d - d_s)$ and $R_x = (d - d_s)$. Substituting these expressions into Equation 3.4 gives:

$$Q = \frac{1.49}{n} W S^{0.5} (d - d_s)^{5/3} \tag{3.5}$$

To obtain a runoff flow rate per unit of surface area, q, Equation 3.5 is divided by the surface area of the sub-catchment, A (which should not be confused with the cross-section area A_x through which the runoff passes):

$$Q = \frac{1.49}{A.n} W S^{0.5} (d - d_s)^{5/3} \tag{3.6}$$

Substituting this equation into the original mass balance relation Equation 3.5 results in:

$$\frac{\partial d}{\partial t} = i - e - f - \alpha (d - d_s)^{5/3} \tag{3.7}$$

where α is defined as:

$$\alpha = \frac{1.49}{A.n} WS^{0.5} \tag{3.8}$$

Equation 3.5 is an ordinary nonlinear differential equation. For known values of i , e, f, ds and α it can be solved numerically over each time step for ponded depth d. Once d is known, values of the runoff rate q can be found from Equation 3.6.

For each sub-catchment that receives runoff from one or more other sub-catchments, the precipitation rate i for each of its subareas has Q_r / A added to it, where Q_r is the total runoff (CFS) routed onto it from the contributing sub-catchments, as computed at the end of the previous time step, and A is the total surface area of the receiving sub-catchment.

3.1.2 Routing Method

The simplest distributed routing method is the *kinematic-wave* model, which neglects the local acceleration, convective acceleration and pressure terms in the momentum equation for dynamic waves. For open channel flows, the continuity and momentum equation and their combined form for kinematic waves are given as follows:

$$\left.\begin{aligned} &\frac{\partial A}{\partial t} + \frac{\partial Q}{\partial x} = 0 \\ &Q = \alpha A^m \end{aligned}\right\} \qquad \frac{\partial A}{\partial t} + \alpha \frac{\partial \left(A^m\right)}{\partial x} = 0 \tag{3.9}$$

where, Q is the flow rate, A is the channel cross-section area, t is time, x is distance and for *turbulent* flow, α can be calculated by Manning's:

$$\alpha = \frac{1}{n} \frac{\sqrt{S_0}}{P^{2/3}} \quad \text{and} \quad m = \frac{5}{3} \tag{3.10}$$

Where n is the Manning friction coefficient, P is the wetted perimeter and S_0 is the bed slope. For wide rectangular sections (e.g., overland flow) the continuity and momentum equation and their combined form for kinematic waves are given as follows:

$$\left.\begin{aligned} &\frac{\partial y}{\partial t}+\frac{\partial q}{\partial x}=i-f \\ &q=\alpha y^{m} \end{aligned}\right\} \qquad \frac{\partial y}{\partial t}+\alpha\frac{\partial\left(y^{m}\right)}{\partial x}=i-f \tag{3.11}$$

where, for *turbulent* flow, α can be calculated by Manning's:

$$t_c^{\bullet}=\frac{L}{\alpha y_{Lr}{}^{m-1}} \qquad \text{and} \qquad m=\frac{5}{3} \tag{3.12}$$

Here, q is the flow rate per unit width, y is the water depth, i is the rainfall intensity and f is the infiltration rate. By using the momentum equation for overland flow, the celerity (c) of kinematic waves is given by:

$$c=\frac{dq}{dy}=\alpha m y^{m-1}=mV \tag{3.13}$$

Where, V is the water velocity. The time at which the maximum outflow is reached is defined as the time of concentration and given as:

$$t_c=\left(\frac{L i_0{}^{1-m}}{\alpha}\right)^{1/m} \tag{3.14}$$

where L is the distance along the catchment plane and i_0 is spatially constant rainfall excess.

3.2 HEC-RAS:

Water surface profiles are computed from one cross-section to the next by solving the energy equation with an iterative procedure called the standard step method. The energy equation is written as follow:

$$Z_2+Y_2+\frac{a_2V_2{}^2}{2g}=Z_1+Y_1+\frac{a_1V_1{}^2}{2g}+h_e \tag{3.15}$$

Where, Z_2 and Z_1 are elevation of the main channel inverts, Y_1 and Y_2 are the depth of water at cross-sections, V_1 and V_2 are average velocities, a_1 and a_2 are velocity weighting coefficients, g is the gravitational acceleration and h_e is the energy head loss. The energy head loss between two cross-sections is comprised of friction losses and contraction or expansion losses. The equation for the energy head loss is as follows:

$$H_e = L\overline{S_f} + C\left|\frac{a_2 V_2^{\,2}}{2g} - \frac{a_1 V_1^{\,2}}{2g}\right| \tag{3.16}$$

Where L is the discharge weighted reach length, $\overline{S_f}$ is representative friction slope between two sections and C is the expansion or contraction loss coefficient.

The distance weighted reach length is calculated as:

$$L = \frac{L_{lob}\overline{Q}_{lob} + L_{ch}\overline{Q}_{ch} + L_{rob}\overline{Q}_{rob}}{\overline{Q}_{lob} + \overline{Q}_{ch} + \overline{Q}_{rob}} \tag{3.17}$$

Where lob, ch, rob are representing left overbank, main channel and right overbank respectively.

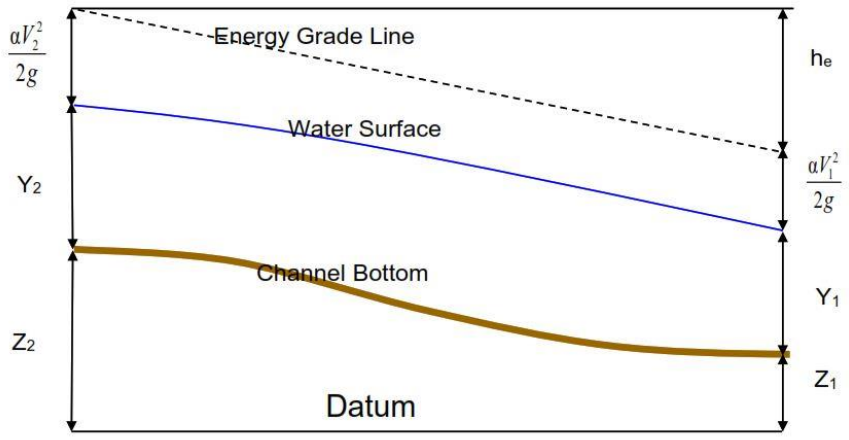

Figure 3.4 Representation of terms in the energy equation.

3.3 CHAMP

There are two different modules of the CHAMP software that can be operated separately to define the flood zone map of an area; (1) Wave Height Analysis for Flood Insurance Studies (*WHAFIS*) and (2) *Run-up*. Before describing each module, flood map zone details have been explained below from theories of (Bellomo, Pajak, and Sparks 1999):

3.3.1 Flood Map Zones

The V Zone is considered to be an area of special flood hazard that is subject to high-velocity wave action from storms or seismic sources. The damage potential within the V Zone is considered to be higher than that of most Special Flood Hazard Areas (SFHA). Therefore, more stringent building codes are applied to structures built in these zones, and insurance rates are set commensurate with the risk.

Although wave crest elevations were not shown on the Flood Insurance Rate Map (FIRM), the 3-foot wave criteria were used to delineate the inland limit of the V Zone, which was mostly a function of the 1% annual chance still water elevation. These still-water elevations, which consisted of the astronomical tide and storm surge, were published as regulatory Base (1% annual chance) Flood Elevations (BFEs) within V Zones.

FEMA has published BFEs that was composed of the estimated 1% annual chance storm surge elevation (still-water elevation) plus an estimated wave crest elevation. Figure 5 is a schematic of the wave component of the BFE in coastal areas. Notice that 70% of the computed wave height is added to the still-water elevation to determine the BFE.

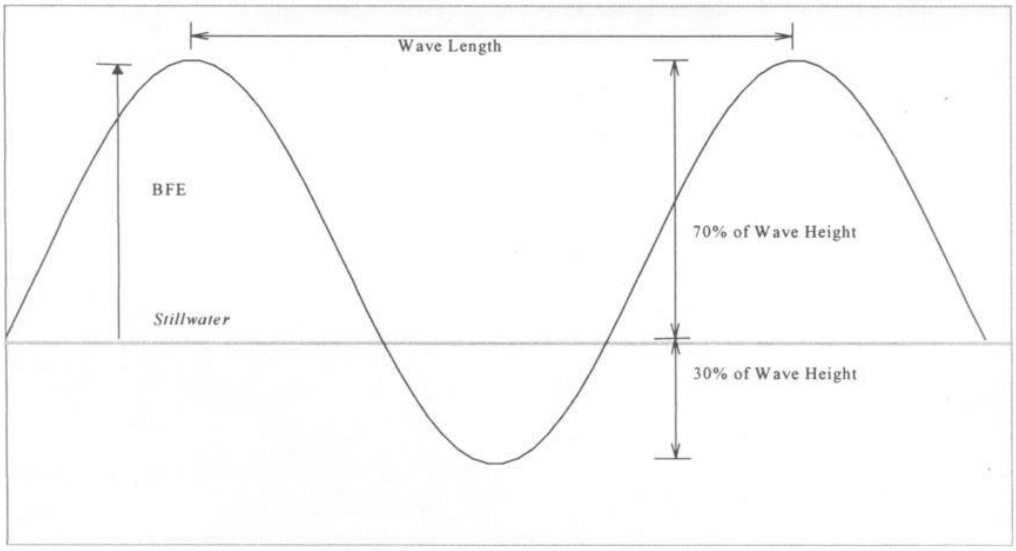

Figure 0.5 Wave crest component of the base flood elevation.

The current guidance for mapping V Zones is to locate and map the most landward of the following three points (FEMA, 1995):

The point where a 3-foot wave height may occur (solved by WHAFIS);

The point where the eroded ground profile (or non-eroded profile, if applicable) is 3 feet below the computed wave runup elevation (solved by Run-Up); and

The inland limit of the primary frontal dune as defined in the national flood insurance program (NFIP) regulations.

3.3.2 WHAFIS Module

The WHAFIS module only solves the equations to determine the wave heights based on the offshore wave characteristics and water depth in flooded areas, considering the tide range and wave setup. The inputs of software are bathymetry, storm and waves characteristic, land cover and ocean fetch size.

The approximate conservation of wave action equation governing wave height variation along a wave transect, neglecting mean current velocity and refraction effect is:

$$\frac{\partial}{\partial x}\left(\frac{c_g E}{\Omega}\right)=\frac{W_{net}-E_P}{\Omega} \tag{3.18}$$

Where E is the time-averaged total wave energy per unit area, c_g is wave group velocity, Ω is angular frequency and equal to ($\frac{2\pi}{T}$), T is spectral peak wave period, W_{net} is time-averaged rate of net wind energy input per unit area, E_p is time-averaged rate of energy dissipation per unit area due to plants and x is distance along the transect. W_{net} includes the effect of wind energy input, wave "white-capping", wave-wave interaction and bottom friction.

Expanding the derivative on the left side of Equation 18 and using $\Omega=\frac{2\pi}{T}$, the conservation of wave equation can be expressed as:

$$\left(c_g T\right)\frac{\partial E}{\partial x}+E\frac{\partial\left(C_g T\right)}{\partial x}=TW_{net}-TE_P \tag{3.19}$$

This is the governing equation used for solving the wave heights along a wave transect. The source term W_{net} is determined by using approximate differential forms of the "shallow water" wave height and wave period growth equations in the U.S. Army Shore Protection Manual (SPM 1984).

The conservation of waves equation stated that, if no new waves are being generated by a local disturbance, the time rate of change of wavenumber (k) is balanced by the spatial rate of change of the angular frequency as below:

$$\frac{\partial k}{\partial t}+\frac{\partial \Omega}{\partial x}=0 \tag{3.20}$$

Omitting the time variation of the wavenumber, and considering the generation of near waves by the local wind, Equation 20 can be modified as:

$$\frac{\partial \Omega}{\partial x} = S \tag{3.21}$$

Where, S is the source term as a function of water depth, wave height, wind speed, and the spectral peak wave period.

3.3.2.1 Wave Energy Density (E)

If hurricane waves were monochromatic, the wave energy density E from Equation 18 would be related to the wave height by:

$$E = \frac{1}{8}\rho g H^2 \tag{3.22}$$

Where ρ is the water density, g is the gravitational acceleration and H is the wave height.

However, monochromatic waves exist only in the laboratory. Real waves have a range of heights and periods, referred to as a "wave spectrum". To account for the shape-preserving characteristic of real spectra, the effective wave height for the spectra should be chosen as the root mean square (RMS) wave height (H_{rms}). H_{rms} is related to the wave energy density in the same manner as Equation 3. 22 but H replaced by H_{rms}:

$$E = \frac{1}{8}\rho g {H_{rms}}^2 \tag{3.23}$$

Rather than directly expressing E in terms of H_{rms}, it is more convenient to express in terms of energy-related wave height, the so-called "zero moment wave height" (H_{m0}). However, H_{rms} is given in terms of H_{m0} by the approximate expression of:

$$H_{rms} = H_{m0} / \sqrt{2} \tag{3.24}$$

H_{m0} is convenient to use since it can be related directly to the "significant wave height" (H_s), which is the average height of the highest $(1/3)$ waves. In deep water H_s and H_{m0} are approximately equal. In shallow water, H_s can be up to 70 percent greater than H_{m0}.

By substituting Equation 3.21 for H_{rms} into Equation 3.23 for E, the following expression is obtained:

$$E = \frac{1}{16} \rho g {H_{m0}}^2 \tag{3.25}$$

Substituting Equation 3.25 into Equation 19 and rearranging, the wave action equation becomes:

$$\left(c_g T\right) \frac{\partial \left(H_{m0}\right)^2}{\partial x} + \left(H_{m0}\right)^2 \frac{\partial \left(C_g T\right)}{\partial x} = \left(\frac{16}{\rho g}\right) \left(TW_{net} - TE_P\right) \tag{3.26}$$

3.3.2.2 Wave Group Velocity (c_g)

The expression used for the wave group velocity (c_g) also depends upon whether monochromatic waves or a spectrum of waves is being modeled. Because the present model is meant to represent a relatively narrow spectrum, c_g is approximately equal to the average group velocity of waves near the spectral peak, which in turn is approximately equal to the group velocity at spectral peak. The approximate expression used to calculate c_g is therefore given as:

$$c_g = \frac{L}{T} \left(\frac{1}{2} + \frac{kd}{\sinh(2kd)} \right) \tag{3.27}$$

Where d is still water depth, L is the local wavelength of waves at spectral peak and equal to:

$$L = \left(\tanh \frac{2\pi d}{L_0} \right)^{1/2} \tag{3.28}$$

And L_0 is the equivalent deepwater wavelength of waves at spectral peak:

$$L_0 = \frac{g}{2\pi} T^2 \tag{3.29}$$

Equation 3.19 for c_g is the same as that for a monochromatic wave, except that the monochromatic wave period has been replaced by the spectral peak wave period. To used Equation 3.27 for c_g, it must be assumed that the wave spectrum being modeled fulfills the "dominant peal" assumption, i.e., the frequency spectrum has one dominant, relatively sharp peak and possibly several considerably smaller secondary peaks. Shallow areas with a water depth of less than 30 feet are the primary interest of this research for calculation of wave height variation. Hurricane spectra for these shallow areas appear to fulfill the "dominant peak" assumption because the shallow water tends to amplify the spectral peak associated with the longest period.

If Equation 19 is rearranged, the equation becomes:

$$c_g T = \frac{L}{2}\left(1 + \frac{2kd}{\sinh(2kd)}\right) = \frac{L}{2}\left(1 + \frac{\lambda}{\sinh \lambda}\right) \tag{3.30}$$

3.3.2.3 Plant-induced Wave Energy Dissipation (E_P)

The wave energy dissipation through marshes is mainly the result of the drag force generated between the marsh plant and the wave current. The total energy dissipation through a

predetermined marsh grass transect segment is also a function of the plant density within the segment and the individual plant geometry.

The plant energy dissipation E_P is the energy dissipated by marsh plants per second over square foot of the ground area at a given point on a transect.

3.3.2.4 Wave Crest Elevation (η)

The National Academy of Science (NAS) recommends approximating η for controlling wave height by the expression:

$$\eta = \mu H_s \tag{3.31}$$

Where $\mu = 0.7$ and η is measured relative to the still water elevation. In general, μ is a function of the local wave period, still water depth, wave height, and bottom slope. It ranges from $\mu = 0.5$ for deep water waves to almost 1.0 for breaking and near-breaking solitary waves. The NAS recommends $\mu = 0.7$ as an average, covering the range of conditions of primary interest to FEMA.

3.3.3 Run-up Module

The Run-up module only solves for the run-up elevation based on the wave characteristics and the land slope, without considering the wave setup and tide range. The criteria of considering an area as a VE zone is the ground profile 3 feet or more below the calculated run-up elevation as shown in Figure 3.6.

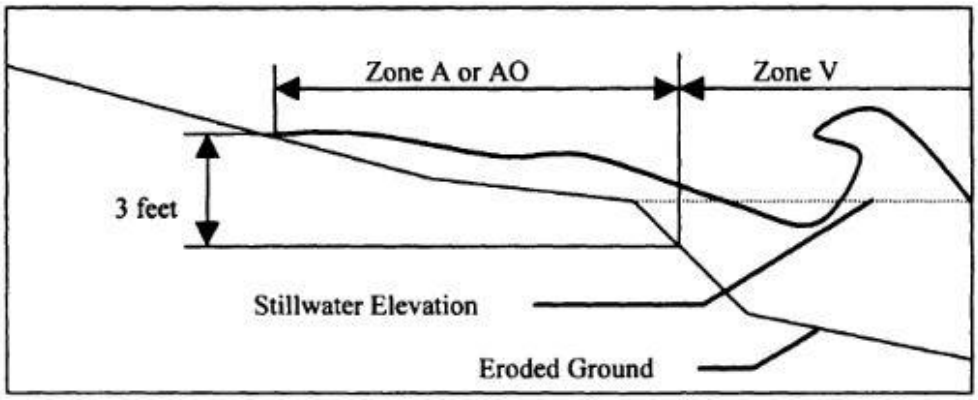

Figure 3.6 Defining the flooding zone based on the run-up phenomenon.

3.3.3.1 Governing Equations

Incident wave runup on natural beaches or barriers is usually expressed in a form originally due to (Hunt 1959) in terms of the so-called *Iribarren* number, ξ, as follows:

$$R = c_m H \xi \tag{3.32}$$

Where R is the vertical run-up, H is the wave heights, c_m is a constant that varies based on the method and user judgment and ξ is the *Irribaren* number which can be expressed as follow:

$$\xi = \frac{m}{\sqrt{H/L}} \tag{3.33}$$

Where, m is the slope of the beach, H and L are wave height and wavelength respectively. The wave characteristics in the Iribarren number can be expressed in terms of deep-water or shallow water characteristics. The wavelength for deep-water and shallow water can be calculated respectively as follow:

$$L_0 = \frac{g}{2\pi} T^2 = 1.56 T^2 \tag{3.34}$$

$$L = T\sqrt{gd} \tag{3.35}$$

For regular waves, several authors have confirmed the utility of ($c_m = 1$) to predict regular wave run-up for mild slopes that produce low ξ values, indicating plunging or spilling waves breaking at the slope (e.g. (Losada and Giménez Curto 1980); (Hughes 2004); (Hsu et al. 2012)). This formula has also been shown to work well for many natural beaches, which are relatively smooth and generally ranged in values of $\xi \leq 2.5$.

For irregular waves, $R_{u2\%}$ is the most common expression to report the run-up, and it is defined as the vertical run-up elevation resulted from the top 2% wave heights of the wave spectrum.

Several authors have suggested and used $c_m = 1.6$ to calculate the $R_{u2\%}$ for the irregular wave conditions for mild slope beaches (e.g. (Ahrens 1981); (Burcharth and Hughes 2002); (EurOtop and Pullen 2007)) and the equation will be as follow:

$$R_{u2\%} = 1.6\frac{\tan\alpha}{\sqrt{H/L}}H \tag{3.36}$$

Where H and L are the wave heights and wave-length at the toe of structure (the wave breaking zone near the shoreline) respectively and α is the slope of the beach.

FEMA used the deep-water wave height and wavelength in its formula to calculate the vertical run-up. In that case the constant of c_m is equal to 0.6 and the equation is as follow:

$$R_{u2\%} = 0.6\frac{\tan\alpha}{\sqrt{H_0/L_0}}H_0 \tag{3.37}$$

Where H_0 and L_0 are the deep-water wave height and wavelength.

There are some other expressions to calculate the run-up such as:

(Wassing 1957): $$R_{u2\%} = 8H_s \tan\alpha \quad (3.38)$$

Or (Mase 1989): $$R_{u2\%} = 1.86H_s\xi^{0.71} \quad (3.39)$$

The two different modules of the CHAMP software can operate separately to define the flood zone map in an area.

The WHAFIS module only solves the equations to determine the wave heights based on the offshore wave characteristics and water depth in flooded areas, considering the tide range and wave setup. The criteria for considering the area as a VE flood zone is the wave heights higher than 3 feet.

The Run-up only solve for the run-up elevation based on the wave characteristics and the land slope, without considering the wave setup and tide range. The criteria of considering an area as a VE zone is the ground profile 3 feet or more below the calculated run-up elevation.

Combining these two criteria to find out the maximum flooded regions give us the final map of the flooding zone (Bellomo, Pajak, and Sparks 1999). Figure 3.7 shows the schematic form of what have explained above, the VE Zone has been determined and placed on the transect.

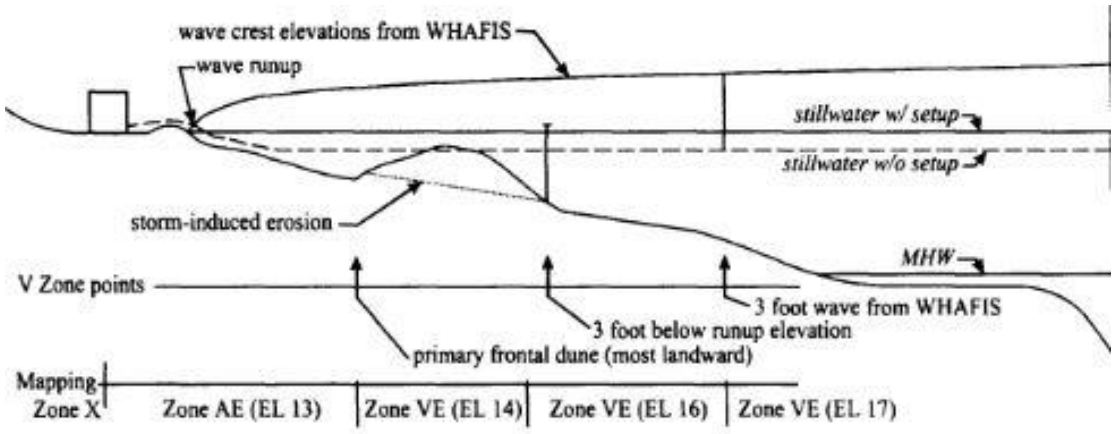

Figure 3.7 Defining the flood zone map based on the combination of WHAFIS, run-up, and erosion.

3.4 MIKE-21

The hydrodynamic model in the MIKE 21 Flow Model (MIKE 21 HD) is a general numerical modeling system for the simulation of water levels and flow in estuaries, bays and coastal areas. It simulates unsteady two-dimensional flows in one-layer (vertically homogeneous) fluids and has been applied in a large number of studies. Flow computation will solve using a depth average model.

The hydrodynamic module of Mike-21 software consists of three equations, the continuity equation and the momentum equations in the horizontal x and y directions. The continuity equation is:

$$\frac{\partial \zeta}{\partial t} + \frac{\partial p}{\partial x} + \frac{\partial q}{\partial y} = \frac{\partial d}{\partial t} \tag{3.40}$$

Where p and q are the flux in x and y direction, d is the time-varying still water depth and ζ is the surface elevation change.

$$\frac{\partial p}{\partial t}+\frac{\partial}{\partial x}\left(\frac{p^2}{h}\right)+\frac{\partial}{\partial y}\left(\frac{pq}{h}\right)+gh\frac{\partial \zeta}{\partial x}+\frac{gh\sqrt{p^2+q^2}}{C^2.h^2}$$
$$-\frac{1}{\rho_w}\left[\frac{\partial}{\partial x}(h\tau_{xx})+\frac{\partial}{\partial y}(h\tau_{xy})\right]-\Omega q-fVV_x+\frac{h}{\rho_w}\frac{\partial}{\partial x}(p_a)=0 \quad (3.41)$$

$$\frac{\partial q}{\partial t}+\frac{\partial}{\partial y}\left(\frac{q^2}{h}\right)+\frac{\partial}{\partial x}\left(\frac{pq}{h}\right)+gh\frac{\partial \zeta}{\partial y}+\frac{gh\sqrt{p^2+q^2}}{C^2.h^2}$$
$$-\frac{1}{\rho_w}\left[\frac{\partial}{\partial y}(h\tau_{yy})+\frac{\partial}{\partial x}(h\tau_{xy})\right]-\Omega p-fVV_y+\frac{h}{\rho_w}\frac{\partial}{\partial y}(p_a)=0 \quad (3.42)$$

Where h is total water depth equal to $(d+\zeta)$, C is the Chezy resistance coefficient, ρ_w is water density, τ is shear stress, Ω is Coriolis parameter (latitude dependence), V is the wind velocity, V_x and V_y are wind velocity parameters, f is wind friction factor and p_a is atmospheric pressure.

The effective shear stresses (τ) in the momentum equations contain momentum fluxes due to turbulence, vertical integration, and sub-grid scale fluctuations. The terms are included using an eddy viscosity formulation to represent sub-grid scale effects. The velocity-based Smagorinsky formula has been applied to calculate eddy viscosity (Rodi 1984).

$$\tau_{xx}=-hE\frac{\partial u}{\partial x} \quad (3.43)$$

$$\tau_{yy}=-hE\frac{\partial \mathrm{v}}{\partial y} \quad (3.44)$$

$$E=C_s{}^2\Delta^2\sqrt{\left(\frac{\partial u}{\partial x}\right)^2+\frac{1}{2}\left(\frac{\partial u}{\partial y}+\frac{\partial v}{\partial x}\right)+\left(\frac{\partial v}{\partial y}\right)^2} \quad (3.45)$$

$$P=h.u \quad (3.46)$$

$$q = h.v \tag{3.47}$$

where u and v are depth-averaged velocity components in the x and y direction respectively and they are related to the flux by Equation 3.46 and 3.47, Δ is the grid spacing and C_s is an empirical Smagorinsky constant that varies between 0.25 and 1.

3.4.1 Wave-Wind Theory

Below there is some formula to find the wave height and period based on the wind field.

$$u_*^{\,2} = C_D.u_{10}^{\,2} \tag{3.48}$$

$$C_D = 0.001 \times (1.1 + 0.039 \times u_{10}) \tag{3.49}$$

Where u_{10} is the wind velocity at the 10m mean sea level, u_* is the shear stress velocity on the surface and C_D is the drag coefficient.

The significant wave heights related to the duration of the wind and fetch size of the sea. If there is enough duration and fetch size, the wave will fully develop, and it can reach its maximum heights corresponding to the wind velocity.

$$t_{x,u} = 77.23 \times \frac{f^{0.67}}{u_*^{\,0.33} \times g^{0.33}} \tag{3.50}$$

Where $t_{x,u}$ is the time to fully transfer the shear stress from the wind to the water surface, f is the fetch size.

If calculated $t_{x,u}$ is less than the t_d (wind duration), the wave height is fetched limited and if $t_{x,u}$ is bigger than t_d, the wave height is duration limited.

I) For fully developed situation:

$$\frac{g.H}{u_*^{\,2}} = 2.11\times10^{2} \tag{3.51}$$

$$\frac{g.T}{u_*} = 2.39\times10^{2} \tag{3.52}$$

II) For the fetch limited situation:

$$\frac{g.T}{u_*} = 2.39\times10^{2} \tag{3.53.}$$

$$\frac{gT}{u_*} = 0.751\times\left(\frac{g.f}{u_*}\right)^{0.33} \tag{3.54}$$

Where H is the wave heights and T is the wave period.

III) For duration limited situation:

$$\frac{g.f}{u_*^{\,2}} = 5.23\times10^{-3}\times\left(\frac{g.t_d}{u_*}\right)^{1.5} \tag{3.55}$$

The new fetch size can be calculated based on wind duration (t_d).

3.5 Compound Flooding

In literature, the most common methods to calculate the co-occurrence probability of sea-level rise and heavy precipitation are the "*Dependence method*" and "*joint-occurrence method*". The dependence between the daily maximum total sea-level or skew surge and discharge time series measures using Kendall's rank correlation (τ) (Kendall 1938). Here is the short description of Kendall's correlation:

Kendall Tau correlation is a non-parametric correlation coefficient to measure the ordinal association between two measured quantities. If the agreement between the two rankings is perfect (i.e., the two rankings are the same) the coefficient has value 1. If the

disagreement between the two rankings is perfect (i.e., one ranking is the reverse of the other) the coefficient has value -1.

If *X* and *Y* are independent, then it is expected the coefficient to be approximately zero.

Let $x_1, ..., x_n$ be a sample for random variable *x* and let $y_1, \ldots, y_n$ be a sample for random variable y of the same size *n*. There are *C*(*n*, 2) possible ways of selecting distinct pairs (x_i, y_i) and (x_j, y_j). For any such assignment of pairs, define each pair as concordant, discordant or neither as follows:

- Concordant if ($x_i > x_j$ and $y_i > y_j$) or ($x_i < x_j$ and $y_i < y_j$)
- Discordant if ($x_i > x_j$ and $y_i < y_j$) or ($x_i < x_j$ and $y_i > y_j$)
- Neither if $x_i = x_j$ or $y_i = y_j$ (i.e. ties are not counted).

Now let *C* = the number of concordant pairs and *D* = the number of discordant pairs. Then define tau as:

$$\tau = \frac{C - D}{C(n, 2)} \tag{3.56}$$

Statistical Significance (Z) can be calculated based on Tau using the formula below:

$$Z = \frac{3 \times \tau \times \sqrt{n(n-1)}}{\sqrt{2(2n+5)}} \tag{3.57}$$

Furthermore, the probability (P-value) can be extracted from the tables based on the Z value.

To facilitate the calculation of $C-D$, it is best to first put all the x data elements in ascending order. For each row of y, we count the number of bigger ranks below the certain rows and insert that number as the concordant value of that row. Based on the same method, the number of smaller ranks below that certain row represents the value of discordant. The summation of the values in the C column is the total concordant and the summation of values in the D column is the total discordant. By following Equation 56, the correlation coefficient can be calculated.

CHAPTER 4

RESEARCH ALGORITHM

4.1 Precipitation Analysis

The map has been extracted from ArcGIS software and applied into SWMM software. The simulation area was conceptually divided into 14 sub-catchments. They could be classified as follows: 7 urban sub-catchments, 5 marsh and wetland sub-catchments, and 2 park and woods sub-catchments.

For undeveloped areas, the sub-catchments border has been chosen based on the basin of the small branches and land use (marsh or forest). For the urban areas, the sub-catchments have been chosen based on the difference in the slope of the land (sections with the same slope considered as a one sub-catchment).

Figure 4.1 shows the simulation map including all the sub-catchments, links and nodes. Links are the channels that can carry the water. The shape of these channels can be defined in the software and they can be represented as rivers, open channels, pipes or sewer lines. The user is able to assign the profile sizes, length, roughness, and slope of these links. Nodes are either the connection point between the links or the outlet of the sub-catchments. The user is able to assign the elevation, maximum depth (which is usually the depth of the following channel) and the ponding area to each node. The length of the links and the area of the sub-catchment areas have been calculated by ImageJ software based on the map scales. The properties of each sub-catchments are presented in Table 4.1. In this study, all the links are natural rectangular open channels that represent rivers and their smaller branches.

The **SCS Rainfall Method** which has developed by the United States Department of Agriculture - Natural Resources Conservation Service (USDA-NRCS) has been used to define precipitation distribution for the study domain. It generated four synthetic 24-hour rainfall distribution curves that cover all geographical regions of the United States. In the SCS Rainfall method, hyetograph distributions Type 1, 1A, 2 and 3 are available and each of these types is applicable for certain regions of the United State. Type II rainfall distribution is the best fit for the State of New Jersey.

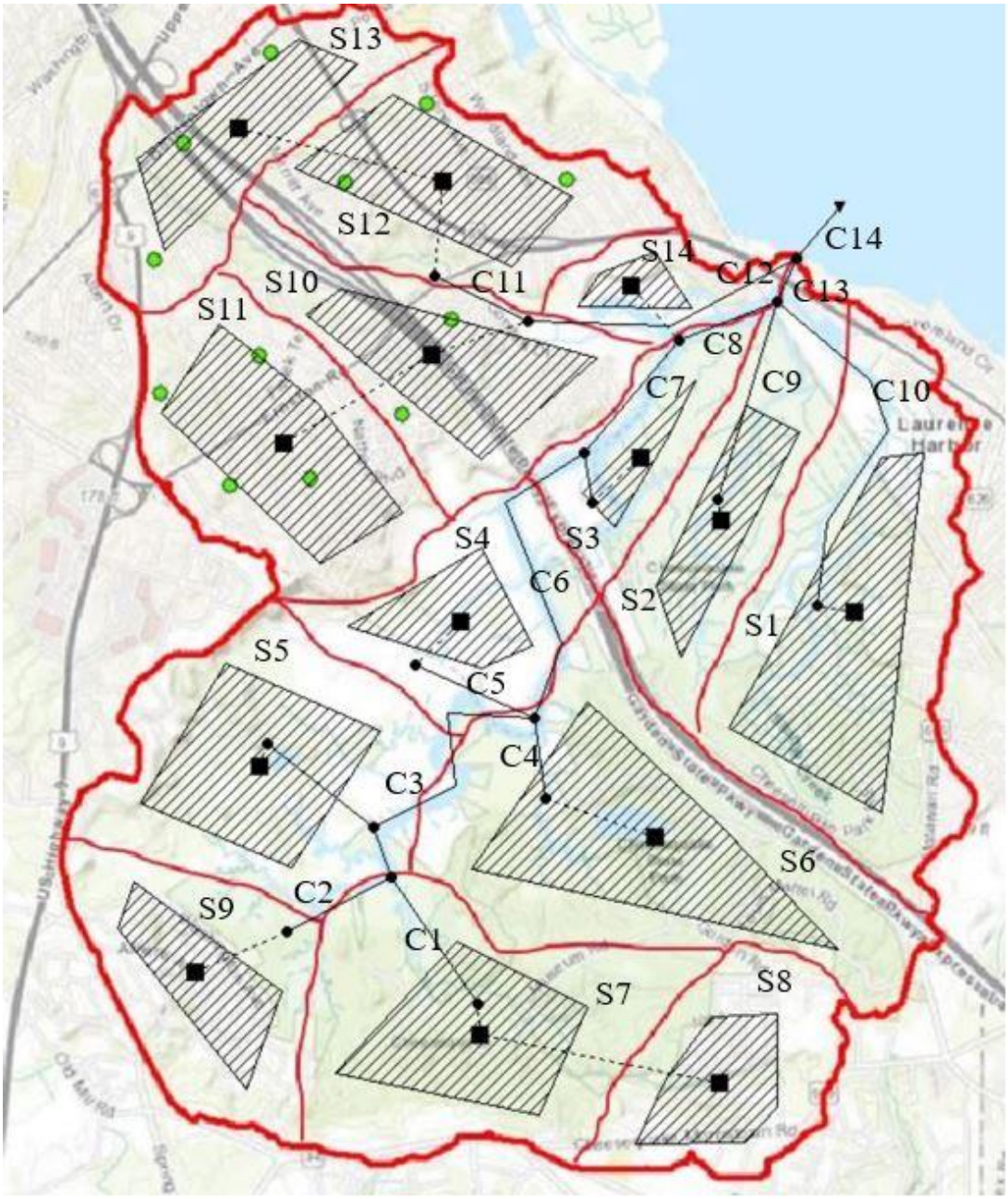

Figure 4.1 Simulation area of the SWWM, including sub-catchments, nodes, channels and outlet. The red lines are the boundary of the sub-catchments.

Table 4.1 Properties of the Sub-Catchments

Sub-Catchment	Area (ac)	Width (ft)	Slope %	Impervious %	Manning's
S1	495	6000	0.5	15	0.3
S2	252	6000	0.1	5	0.3
S3	93	4000	0.1	5	0.3
S4	208	3500	0.1	5	0.3
S5	426	3000	2	7	0.3
S6	454	3000	1	5	0.4
S7	448	2500	3	10	0.4
S8	149	2000	5	50	0.08
S9	200	2000	4	50	0.08
S10	244	4000	2	50	0.08
S11	236	3500	5	50	0.08
S12	249	3000	2	50	0.08
S13	208	3600	5	50	0.08
S14	106	2000	1	50	0.08

The assumptions and strategies to calculate the runoff out of the system and find out the flooding area have been presented below:

4.1.1 Routing Method

In the urban areas, there is no drainage system and the water will flow over the land based on the slope and coverage of the land until it reaches the small branches of Cheesequake creek.

The dynamic wave routing method was used to calculate the runoff. There were no ponding areas in either urban areas or the wetlands.

4.1.2 Manning's Constant

Manning's equation has been used to calculate the water horizontal velocity on the land and in the rivers. There were different manning's constants for different areas. (Kalyanapu, Burian, and McPherson 2010)

For the developed areas, the coefficient was equal to 0.07 (considering medium intensity)

1. For the forest areas, the manning's coefficient was 0.4 (considering mixed forests)
2. For the marsh areas, it was 0.1 (considering woody wetlands)
3. For the river and branches, it was 0.03 (considering natural channels)
4. For the branches in the marsh area, it was 0.05 (a natural channel with vegetation)

4.1.3 Infiltration and Depression Storage

1. The modified Horton method was used to calculate the infiltration of rainwater.

   Three different approaches have been used for three different land use. For the urban areas, the maximum infiltration rate was set equal to 3 in/hr and the minimum infiltration was set at 0.15 in/hr. These numbers have been changes to 4 in/hr and 0.2 in/hr for the forest area respectively. For the marsh and wetland area, since the soil is already saturated, the minimum and maximum infiltration both assigned to be 0.2 in/hr to have the constant and small infiltration in these areas. All the numbers have been extracted from (Hecker 1996).
2. Depression storage was the same for all three types of sub-area. It was 0.5 inches both pervious and impervious areas.

4.2 Inland Flooding

In the first stage, the topography map of the coastal area of the Old Bridge township has been loaded in ArcGIS software. Figure 4.2 shows the topography map of the area of

interest. The HEC-GEORAS extension of ArcGIS software has been used to export the data from the map. Blue line shows the mainstream of Cheesequake creek, red lines are the banks of the river, purple lines are the boundaries of flow path which assigned based on the topography and the green lines are the cross-sections of the river. The data can be extracted at these sections and imported into HEC-RAS software.

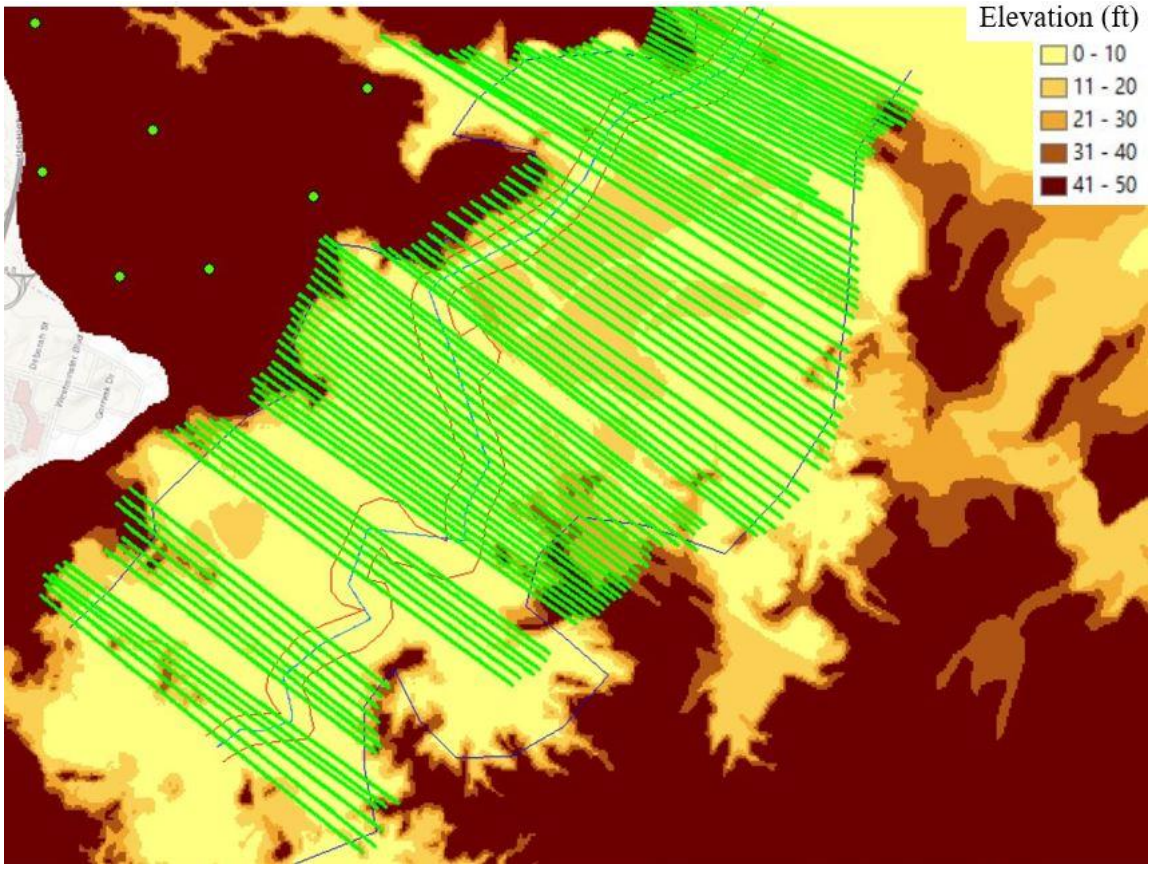

Figure 4.2 Topography map of the domain. Green lines are the sections, the blue line is the mainstream and the red line is the banks of the river.

The land use map has been extracted from the National Land Cover Database (NLCD) website and added to our simulation. Figure 4.3 shows the land use of the simulation area. As can be seen, the main creek can be considered as open water and the rest of the areas are the combination of “woody wetland” and “Emergent herbaceous wetlands”. Based on natural resource conservation service (NRCS), the manning’s

coefficient for the woody wetland is 0.045-0.15 and for herbaceous wetland is 0.05-0.085. therefore, Manning's coefficient of 0.08 has been chosen as a number in between for the bank. Furthermore, manning's coefficient has been set to 0.03 for the main channel.

After importing data into HEC-RAS software, all the data can be read by software and all the elevation data, bank data and stream data will be assigned to the project. Figure. 4.4 shows the imported data into the HEC-RAS. Since the software is sensitive about the distance between the cross-sections, many other sections have been linearly interpolated in software. The typical distance between the section from ArcGIS was about 150ft and new sections have been interpolated for a maximum distance of 40ft between each cross-section. The label of sections can be seen in the picture.

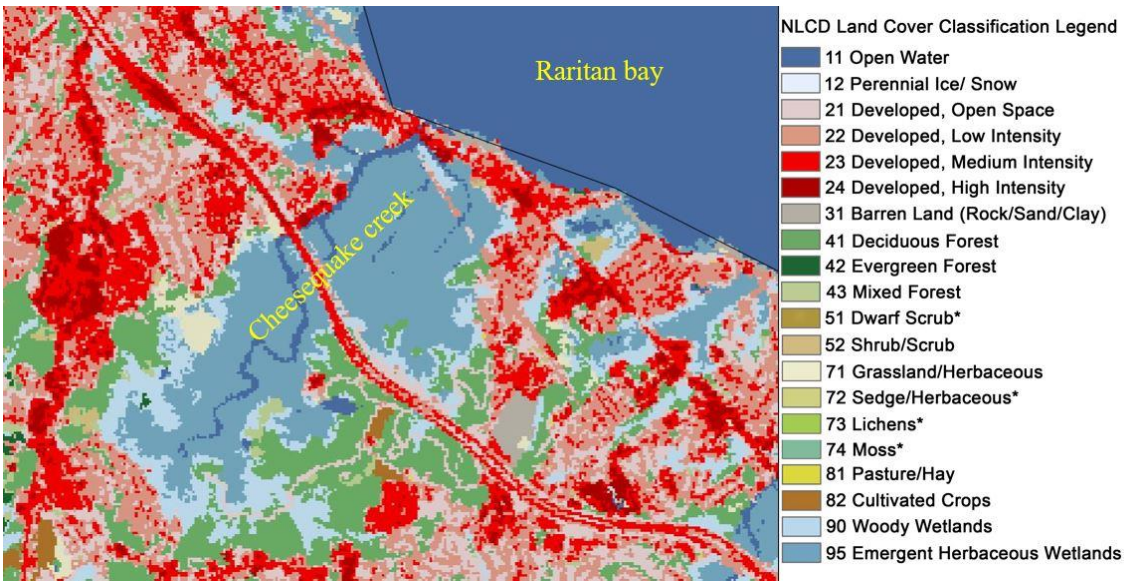

Figure 40.3 Land use of the simulation area from the National Land Cover Database (NLCD) website.

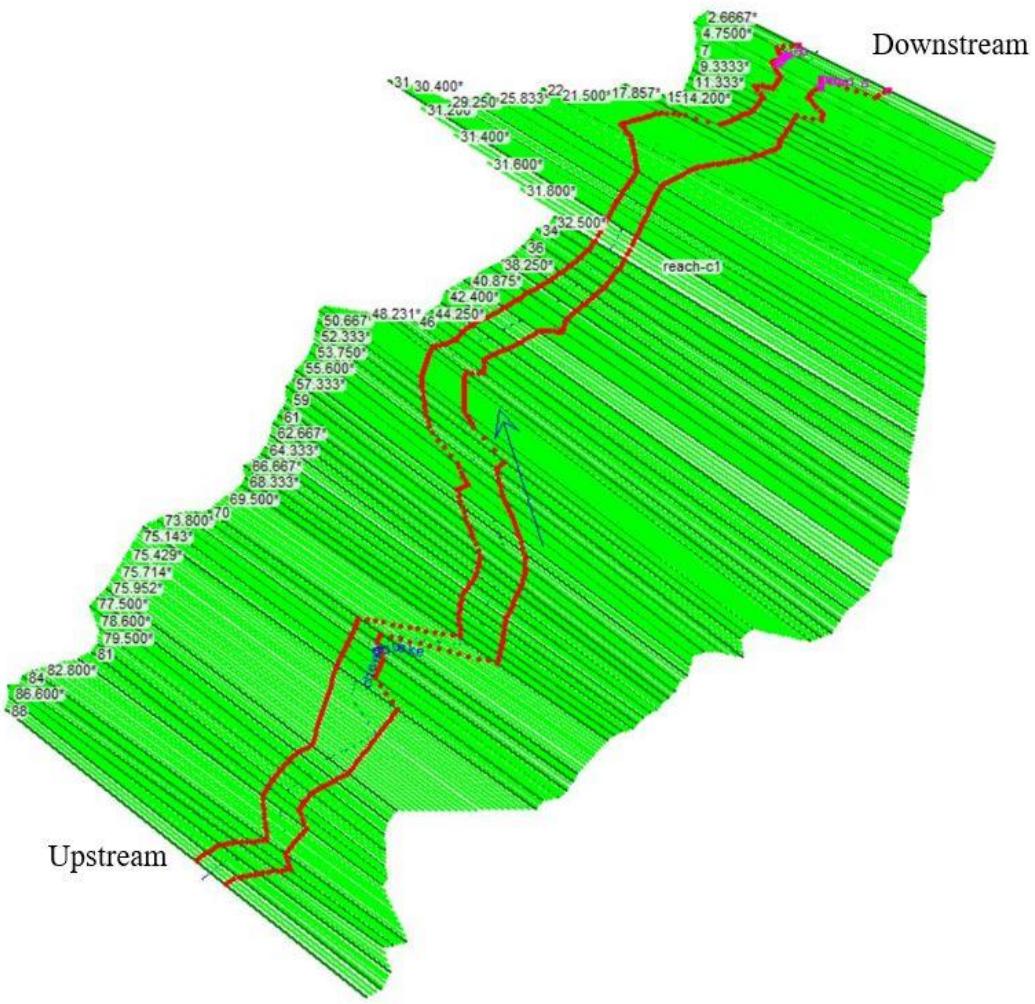

Figure 40.4 Plan of the river in the HEC-RAS. The black lines are the extracted sections from ArcGIS and green lines are interpolated section by software.

Based on the width, depth and water velocity of Cheesequake Creek, the Baseflow of 1000 CFS has been estimated for the creek and the model has been run for steady-state flow mode.

Then, the results extracted from SWWM software has been added to the river as storm data. The maximum flow rate of 7500 CFS has assigned to the Creek and the model has been run for the steady-state mode to calculate the water level rise in the river and find out the flooded areas around the river.

4.3 Ocean Flooding

The bathymetry of Raritan bay has been extracted from the NJDEP website and converted into the ArcGIS file. Figure 4.5 shows the bathymetry of the bay. The elevation of the chosen points in Figure 4.5 has been extracted from the software to transfer the bathymetry data to CHAMP software. Figure 4.6 shows the topography of the coastal areas and the chosen point of the profile. The points start from the inlet of the creek to the middle of the urban area to complete the land part of the profile for CHAMP.

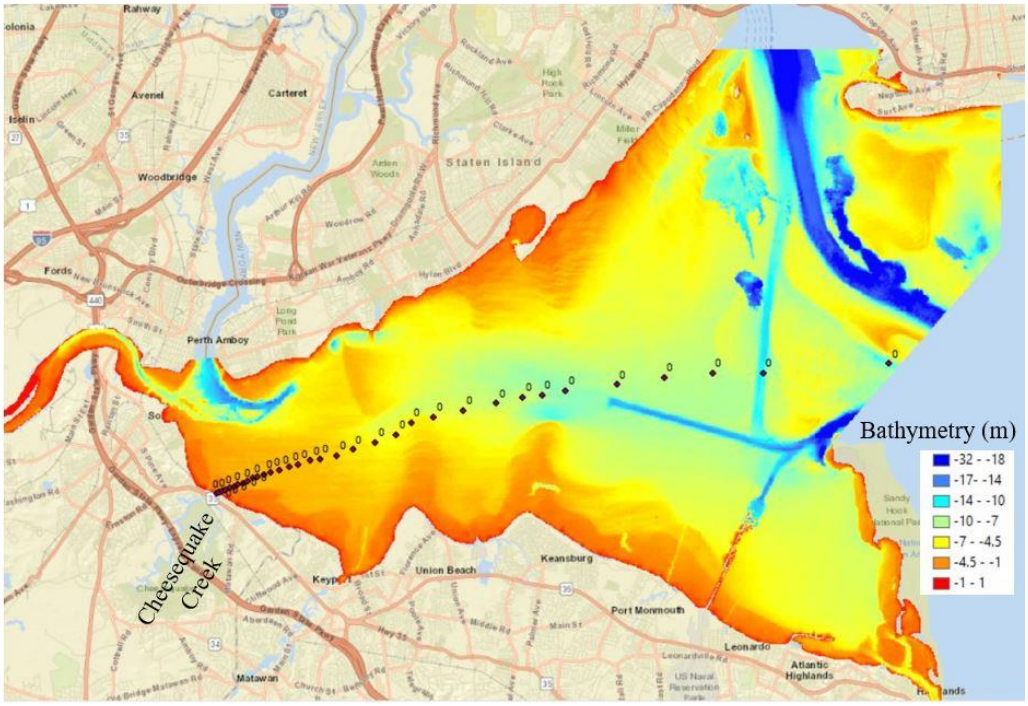

Figure 04.5 Bathymetry of Raritan bay. Black points are the extracted elevation for the CHAMP profile.

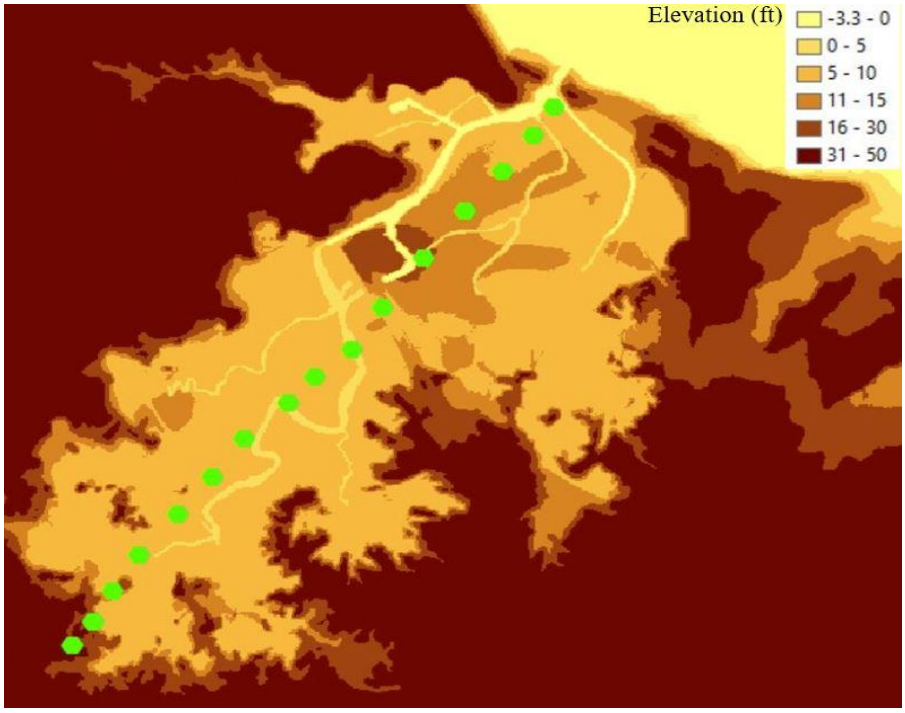

Figure 4.6 The topography of Old Bridge coastal areas. Green points are the extracted points for the CHAMP profile. The points start from the inlet of the creek to the middle of the urban area.

The extracted bathymetry from the bay and topography elevations from the land has merged together to give us the final profile of CHAMP. Since the flooding from the ocean into the land is the main interest of research, the simulation area starts from 10000 ft in the ocean and continue to 14000 ft inland.

Hurricane Sandy has been considered as 100-years return period of the simulation domain. Therefore, the data of the storm has been extracted from the NOAA website to be used as the boundary condition of the model. Mean sea-level rise during Hurricane Sandy was about 13.2 ft. The elevation of high tide is about 6 ft in Raritan bay. The significant wave heights of 20 ft have been recorded during Hurricane Sandy and the corresponding period of these waves was around 14 seconds. The model has been run for mentioned conditions and the flood zone map (including AE and VE zone and LIMWA line) has been

presented for the study domain. Also, the effect of vegetation has been assessed in the protection of urban areas behind the marsh zone.

4.3.1 Vegetation Effect

It is found that the impact of bathymetry is largest for storms with lower flood levels, due to wave breaking on the shoreline. However, the role of the marsh plants grows larger for storms with higher flood levels, when wave breaking does not occur and the vegetative drag becomes the main source of energy dissipation. (Marsooli, Orton, and Mellor 2017) have shown that the marsh vegetation at Jamaica bay, New York, can decrease the wave height up to 40% in some areas.

Based on (FEMA 2015) guideline, different land use can be assigned to each computational area in WHAFIS. There is land used called “vegetation height” which is a perfect match with land cover of the area of our interest. This land use is covered by flexible marsh vegetation which can oscillate with the waves. Based on the storm surge elevation and vegetation heights, this vegetation can be submerged or emerged. The software calculates the drag force based on the vegetation height, diameter and spacing between the plants. There is another option to choose the area of interest and the type of vegetation and the software will fill the parameter based on the default values.

The area of interest has been chosen as “Mid-Atlantic” and the plant type has been chosen as “tall salt meadow cordgrass”. The height of the plant is about 5 ft based on the field observation and the rest of the parameter left blank to be filled by software based on the plant type and its heights (diameter, spacing, drag coefficient). Considering the storm surge which increases the water level up to 15ft, these 5 ft plants are fully submerged.

4.4 Compound Flooding

In our study method, the joint probability of compound flooding didn't calculate by the statistical method. Instead, it has been assumed that the compound flooding will happen in this area and the main focus of the study is to predict the magnitude of flooding based on co-occurrence of both events.

There are three mechanisms that can happen in the co-occurrence of storm surge and precipitation:

(1) In estuarine regions, the joint occurrence of both may elevate water levels to a point where flooding is initiated, or its impacts exacerbated.

(2) Occurs when a destructive storm surge already causes widespread flooding, such that any significant rainfall on top of this (even if it is not an extreme event on its own) increases the flood depth and/or extent of the inundated area.

(3) Occurs during a moderate storm surge that does not directly cause flooding but is high enough to fully block or slow down gravity-fed stormwater drainage, such that precipitation is more likely to cause flooding.

To find out the joint probability of these two event, search for the highest annual storm surge, and then take the highest precipitation within a time range of 1-2 days of this event (covers mechanisms (1) and (2)), or search for the highest annual precipitation, and then take the highest storm surge within a time range of 1-2 days (covers mechanism (3)).

In the study domain, the effect of the third mechanism has already considered since the biggest part of the domain is either rivers or wetlands and the infiltration is almost zero in these areas.

The first and second mechanisms will be assessed in our study domain using the MIKE-21 software.

Therefore, the modeling of Cheesequake Creek has been conducted in MIKE-21 software to investigate the combination of offshore storms and flow from the river. The area of the modeling domain is 6km*6km and the Bathymetry of the domain has been created based on the Arc-GIS maps. The size of each cell is 30m and there are 200 nodes in each direction (total 40000 nodes). Figure 4.7 shows the bathymetry of the study domain.

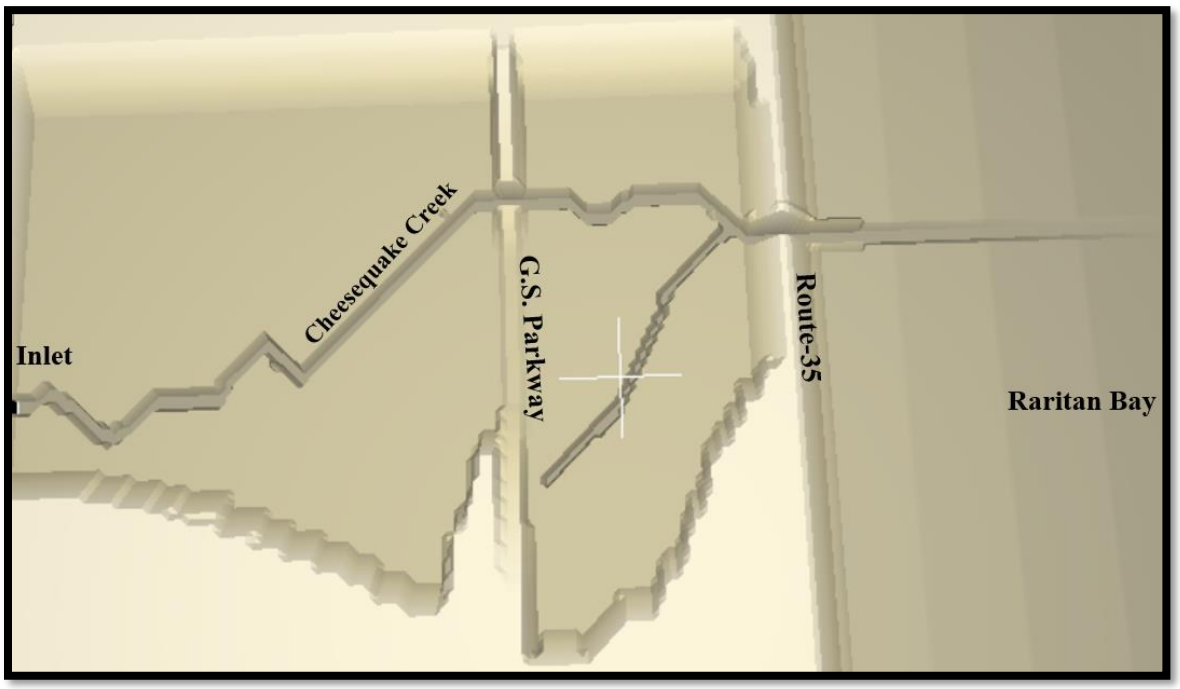

Figure 4.7 Bathymetry of the study domain.

The HD module of MIKE-21 software has been used for these sets of modeling. The time-steps of all modeling were set to 1 second and the simulation continued until it reaches a steady-state. The elevation of 10 m MSL has been chosen as the land elevation and the areas higher than this elevation does not account in the simulation. The lower elevations are vulnerable to the inland flooding. The northern and southern boundary of the model has been set to the *wall*, therefore both of them are no flux boundary. The eastern

boundary has been set to the *wall* to expect the inlet of the river. The inlet of the river has been set to the flux boundary and the value of the flux was 200 m3/s for the 100-year return period precipitation. The eastern boundary of the domain has been set to time-series of water elevation which has been extracted from NOAA website during Hurricane Sandy. Figure 4.8 shows the water level change during Hurricane Sandy in a station close to the study domain.

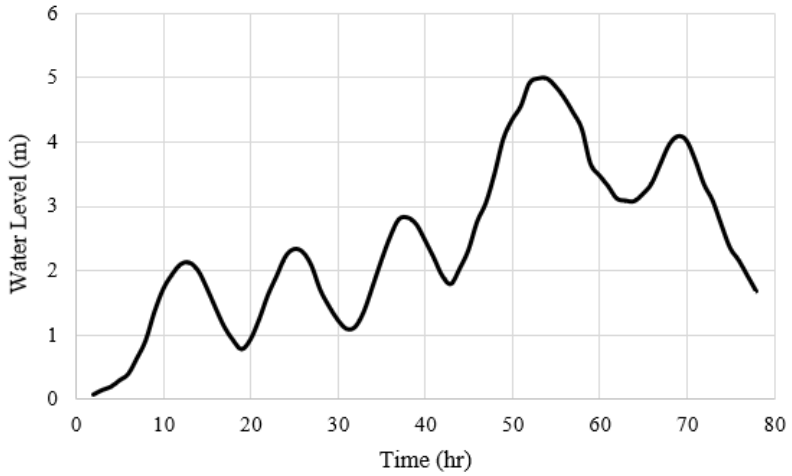

Figure 4.8 Water level change during Hurricane Sandy outside the simulation domain.

The infiltration assumed to be zero since it's already considered in SWMM software. For eddy viscosity, the velocity-based Smagorinsky formula has been exploited with a constant of 0.28 which follows the literature. Also, the different bed resistance for each cell of the domain has been considered to fulfill the requirement for different Manning's coefficient for the main channel and marsh areas.

The simulations have been conducted in three steps:

1) Only river flow,

2) Only offshore storm,

3) Combination of both of them happening at the same time.

CHAPTER 5

RESULTS

5.1 SWMM

Considering the SCS 24-hours 100-year type II flood event (Figure 5.1 shows the rainfall distribution), the model has been run for 48 hours to obtain the response of the system to this rain event.

The outflow of the system divided into the outflow of the drainage system in urban areas and runoff in wetland areas, and it takes about 30 hours to drain all the water from the system.

As shown in Figure 5.2, the urban areas have a quicker response to the rain event, with regard to the smaller Manning's equation on developed areas and the peak of the flow out of the urban areas is higher than the wetlands. Wetlands have a slower response to the rain event and a much smoother flow rate diagram compare to the urban areas. The total volume of water out of urban areas is about 25 million CFS and the total outflow of undeveloped areas are is about 44 million CFS. Since the area of undeveloped parts is about 2.7 times of the urban areas, these numbers make a perfect sense, considering the higher impervious areas in urban parts and higher infiltration rates in the forests.

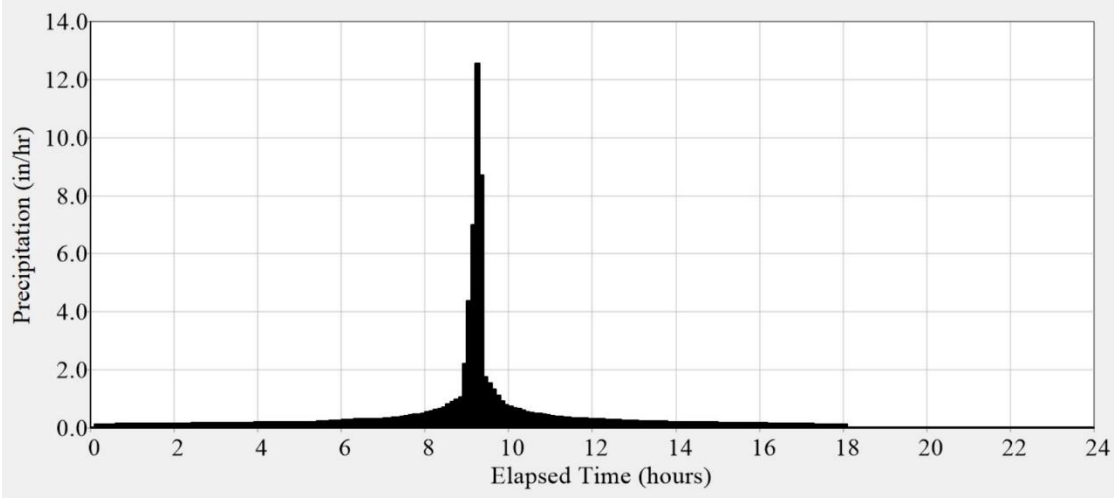

Figure 5.1 SCS 24-hour 100-year type II flooding event over the system as a function of time.

Figure 5.3 shows the total outflow of the system in the mouth of the watershed. The peak of the flow rate is about 6500 CFS and it happens around 10 hours after the rain starts.

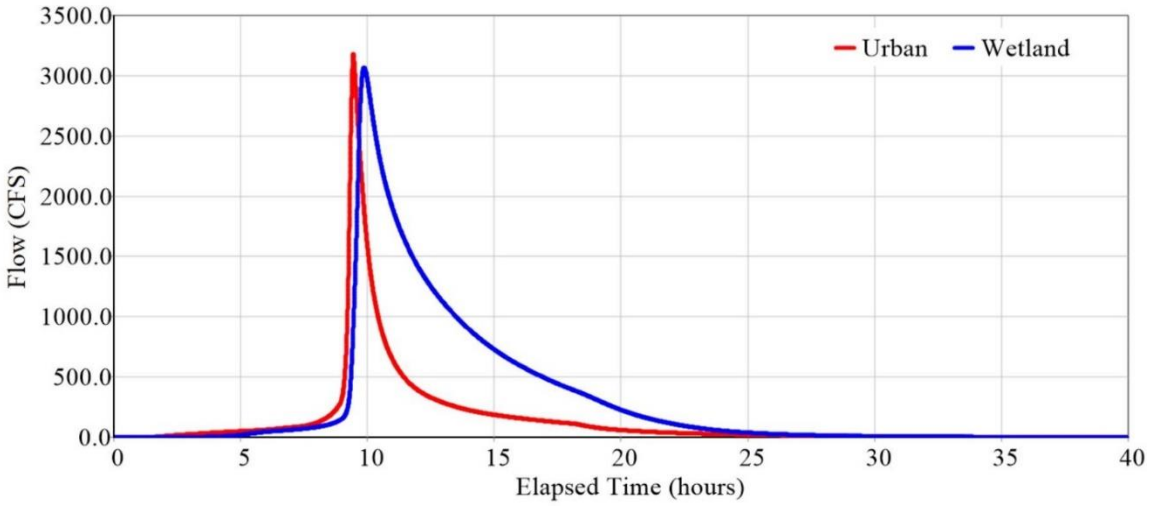

Figure 5.2 Flow rate out of the urban and wetland areas as a function of time at the mouth of the watershed.

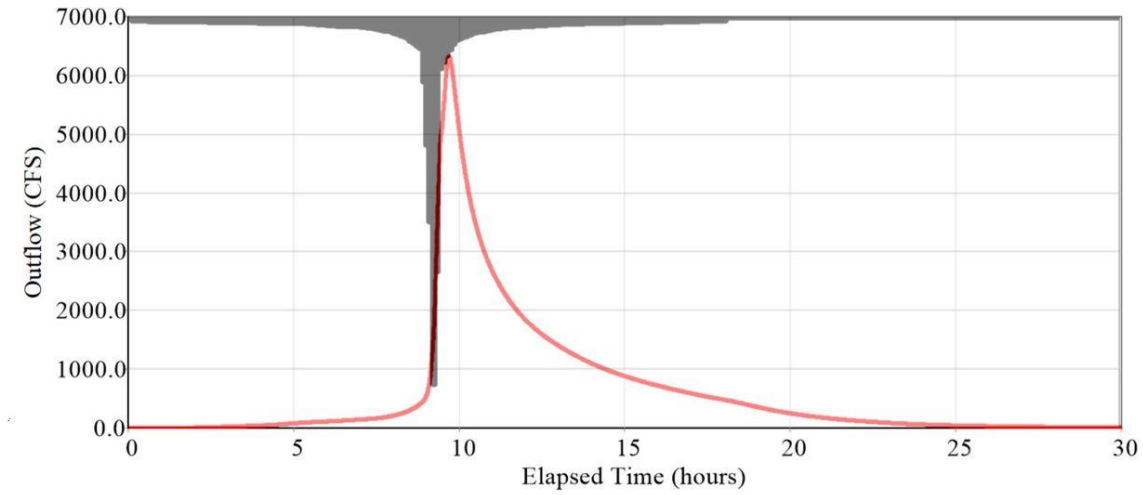

Figure 5.3 Total outflow of the system as a function of time at the mouth of the watershed (where Cheese quake creek meets the Raritan bay). The grey diagram shows the precipitation of the system.

Figure 5.4 shows the total infiltration of the system. By calculating the area underneath the graph, the total infiltered water is about 3.6 inches out of the total rainfall of 8.5 inches.

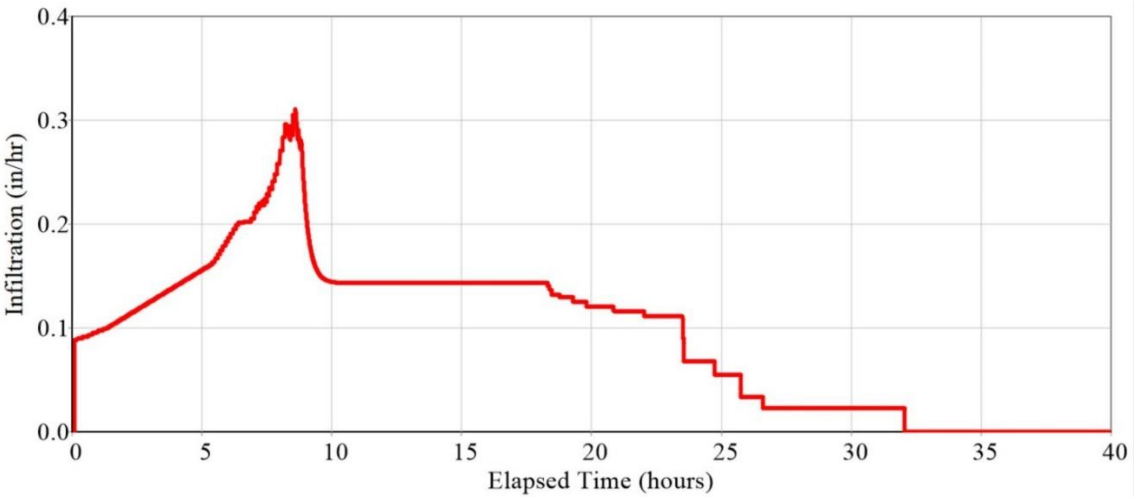

Figure 5.4 Total infiltration of the system as a function of time.

5.2 HEC-RAS

The results extracted from SWWM software has been added to the river as storm data. The maximum flow rate of 6500 CFS has assigned to the Creek and the effect of this storm on the water level and velocity has been determined. The width of the channel varied from 150ft to 450ft, but for most of the cross-sections, it's about 250ft. This variation in the width of the river causes a continuous water elevation change in the channel as shown in the figures below.

Figure 5.5 shows the water level before and after the storm at upstream and downstream of the creek.

Figure 5.6 shows four different cross-sections along the creek after the storm. Cross-sections 1, 30, 50 and 88 have been shown in the image and the location of each cross-section can be found in Figure 4.4. Considering the color bar on the right side of the figures, the velocity of streams can be very different based on the depth and width of the channel. There can be flow division based on the topography of area (second image) and in some cases water can’t flow in parallel channels in the presence of levees (first image).

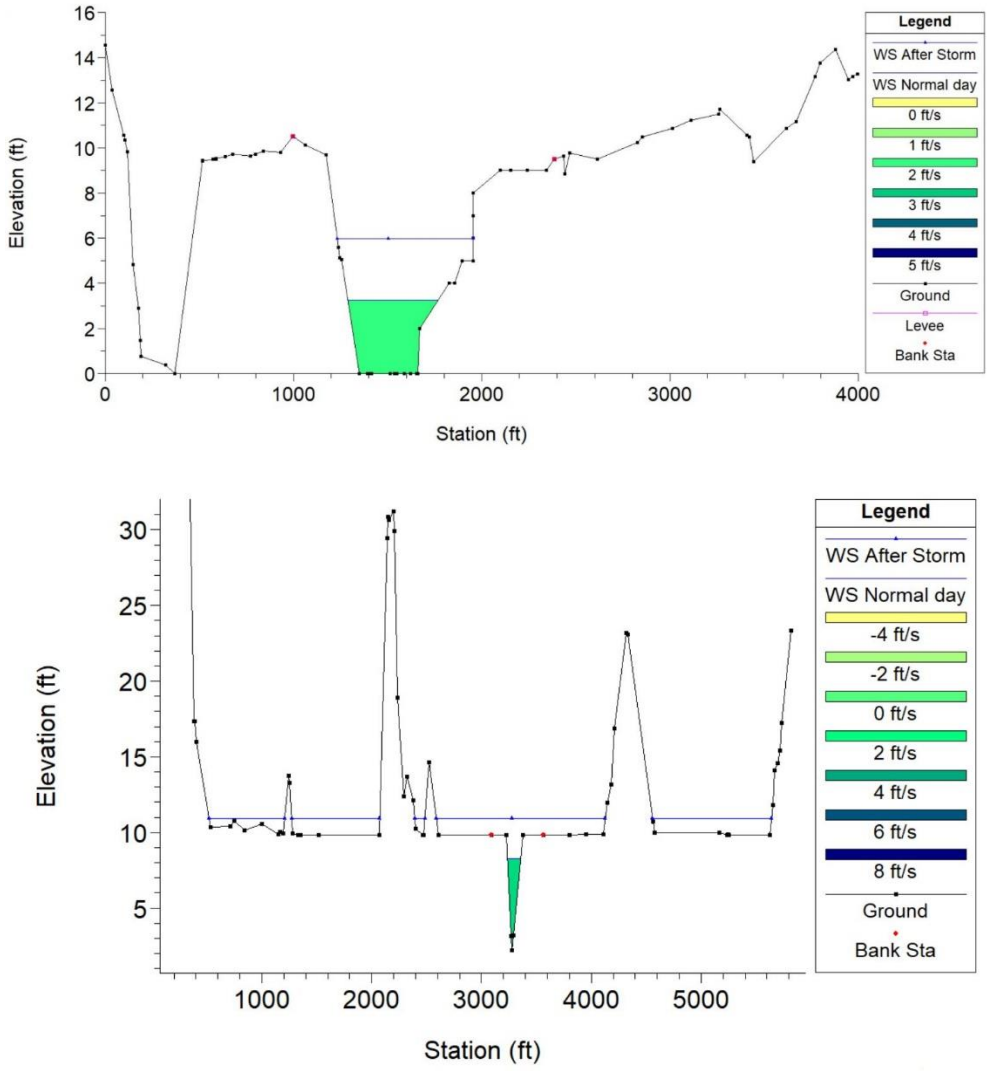

Figure 5.5 Water level before and after the storm. The blue line is the water elevation after the storm. The top image is the mouth of the creek into Raritan bay and the bottom image is upstream of the creek.

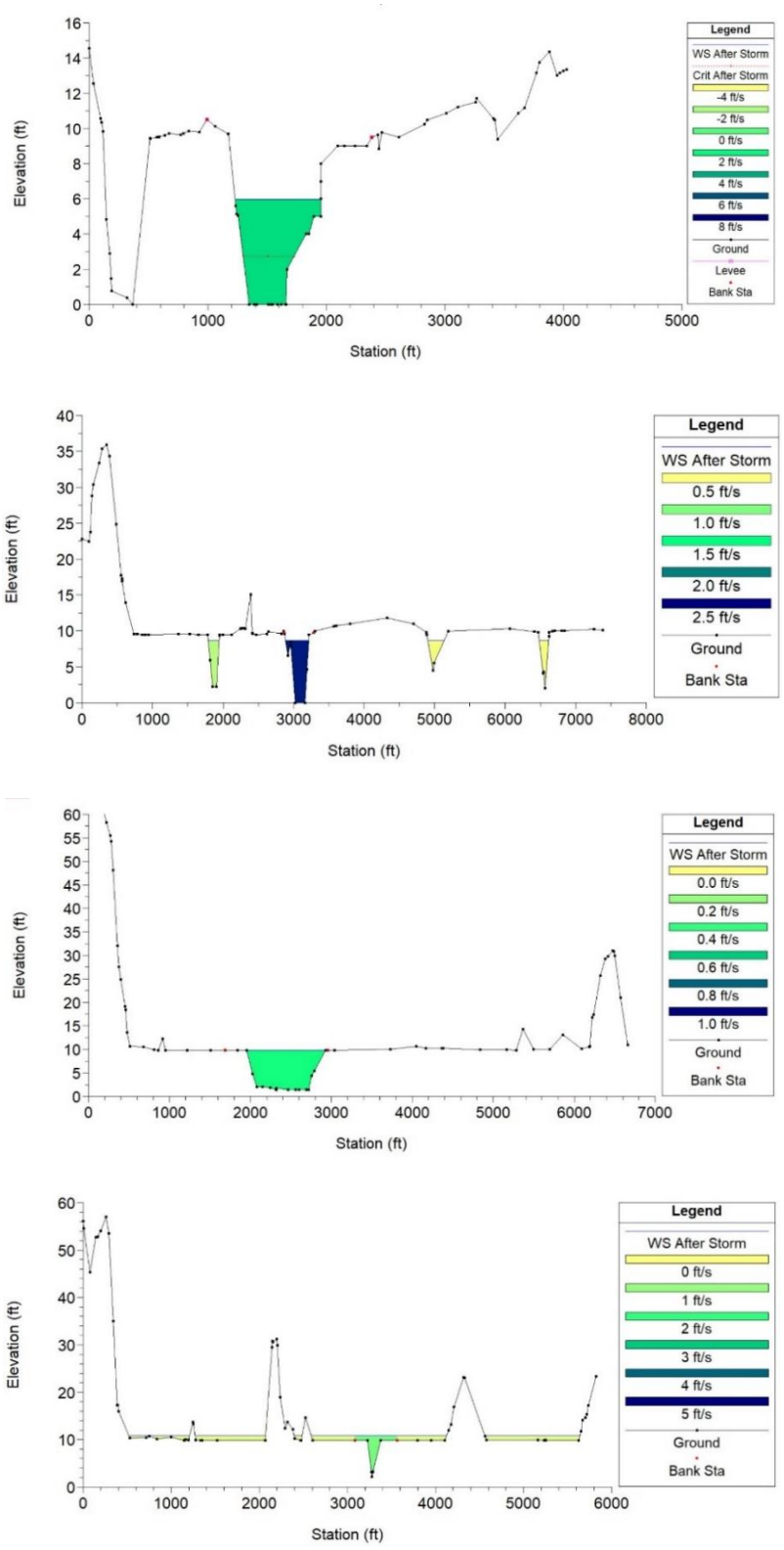

Figure 5.6 Water velocity at four different cross-sections of the creek after the storm. Cross-sections are respectively 1, 30, 50 and 88.

Figure 5.7 shows the plan view of the simulation areas before and after the storm. Based on the topography of the area, the downstream part of the creek is a marsh area that is always flooded but after the storm, the upstream lands are getting flooded too and the water elevation in the downstream area will increase about 3 ft.

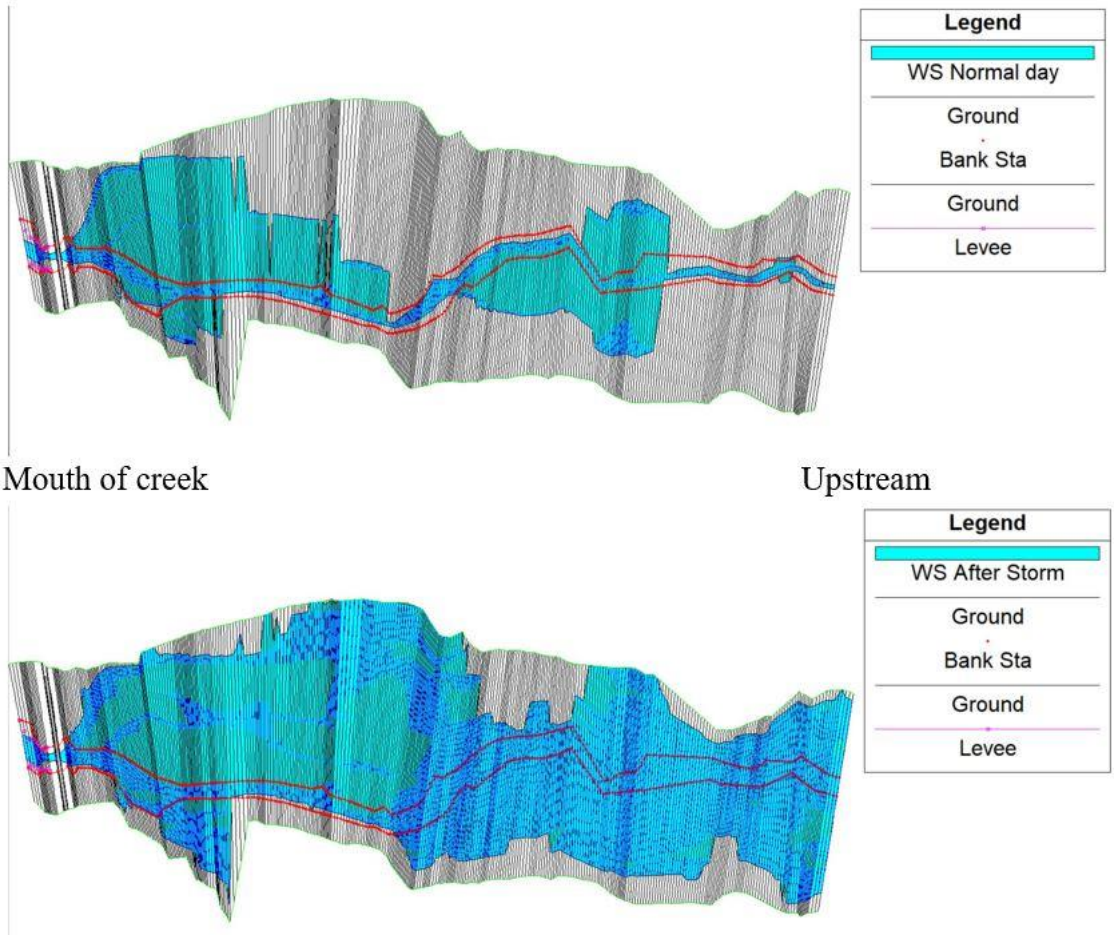

Figure 5.7 Plan view of the simulation areas before and after the storm.

Figure 5.8 is the horizontal profile along the river in both scenarios. It shows that the water level will increase between 3 to 4 ft after the storm alongside the river.

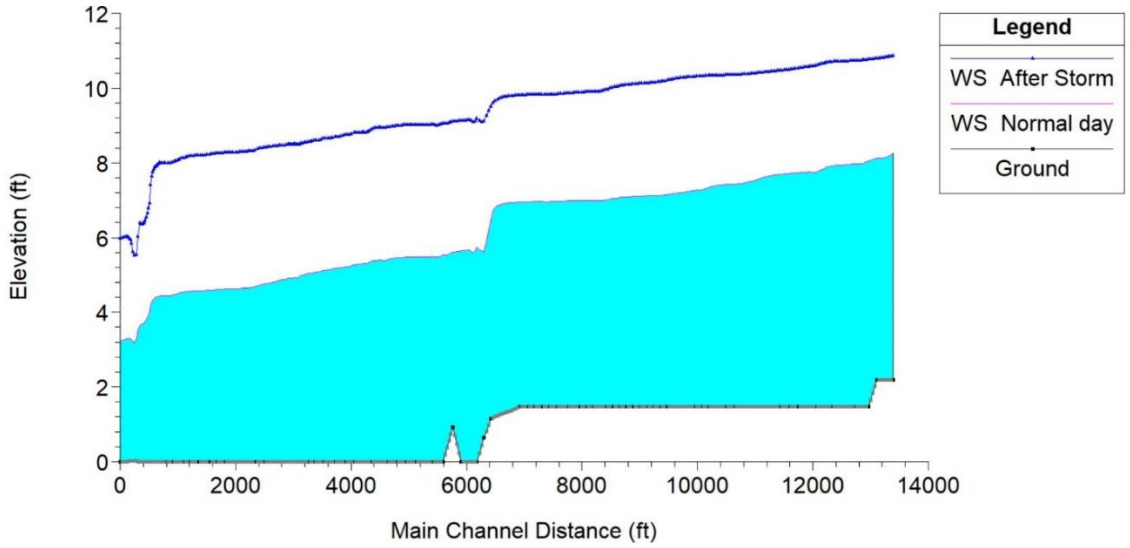

Figure 5.8 horizontal profile along the river before and after the storm.

Figure 5.9 shows the Route 35 bridge over the creek. Comparing the bridge cross-section with other cross-sections demonstrate that, the narrower water path has a significant effect on water velocity, and it has increased up to 9 ft/s under the bridge.

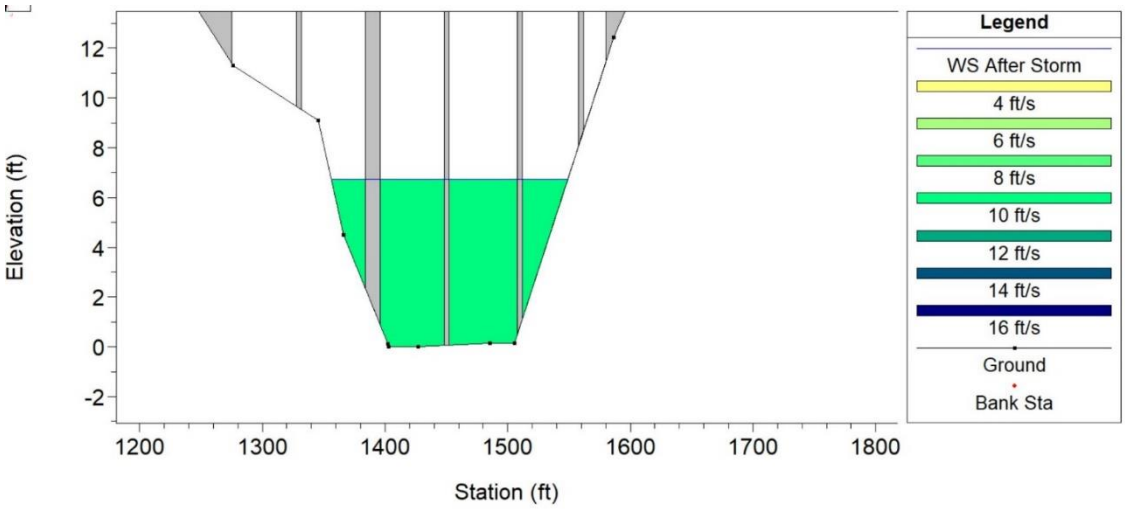

Figure 05.9 Cross-section of Route 35 bridge over the creek. The narrower water path, higher elevation of bank and faster water velocity are the important points of this cross-section. The upper panel is the first cross-section of the bridge and the lower panel is the final section of the bridge.

5.2.1 Levees

To evaluate the effect of the wetland around the main river on mitigation of flooding, the 25 ft high levees have been designed along the river to make sure all the water will remain in the channel. Figure 5.10 shows a levee layout at a random cross-section. The blue line is the water level rise after the storm.

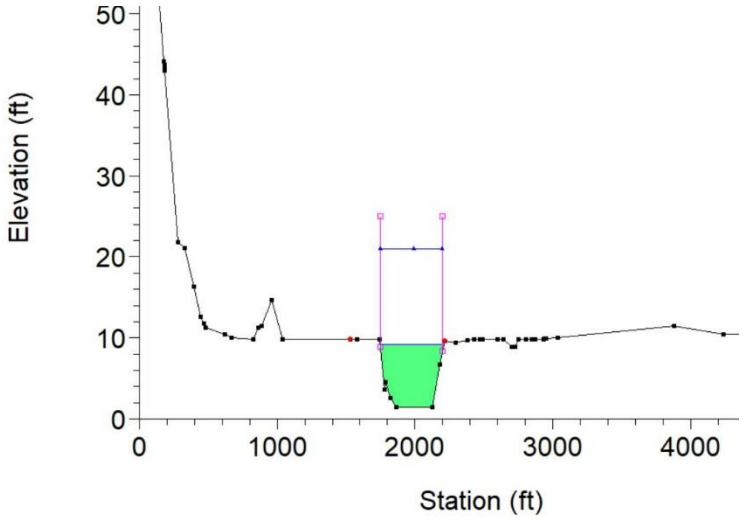

Figure 5.10 Levee layout at a random cross-section.

Since the watershed of the study domain is pretty small compared to most of the watershed, the flow rate of 27000 CFS (considering 3-times bigger domain) has been considered to evaluate the effect of the watershed size on the water characteristics in the river and wetland.

Figure 5.11 shows the birds-eye view of the domain. The pink lines are the levees on 2 sides of the river. The mouth of the bridge is on the left side and the bridge has been highlighted with grey color. Accumulated water can be observed behind the bridge.

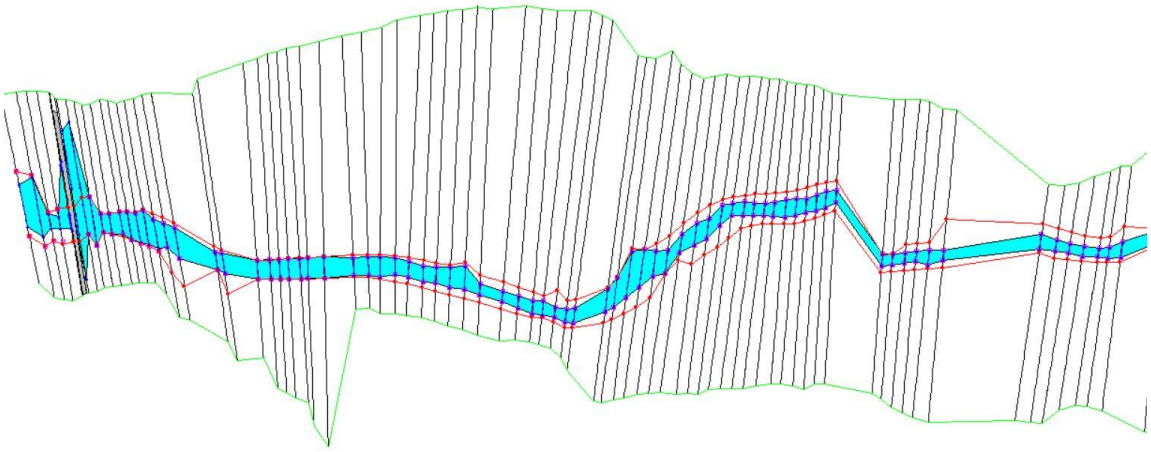

Figure 5.11 Top view of the study domain. The mouth of the river is on the left side and the bridge is highlighted with grey color.

Figure 5.12 shows the water level rise in the river in the presence of the levees and without them. As shown in Figure 5.12, the wetland mitigates the water level from 1 to 3 ft at different locations of the river for a 100-year storm and from 1 to 8 ft for 3-times higher flow rates.

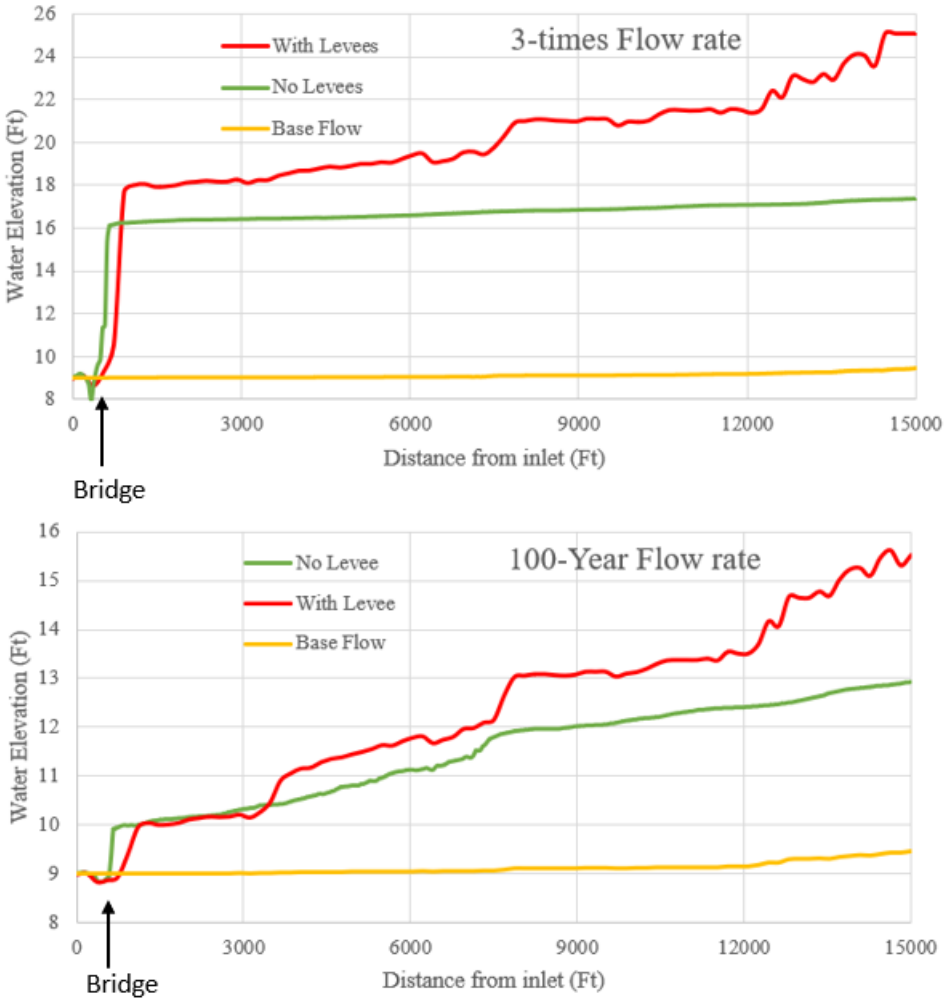

Figure 5.12 Profile of water elevation in case of with levees and without them for flow rates of 9000 and 27000

5.2.2 Backwater of the Bridge

The bridge structures can affect the flow regime in the rivers. Rivers are usually getting narrow close to the bridge cross-section, and the piers of the bridge affects the flow velocity and flow area at that particular cross-section. The contraction of the flow path along the bridge can cause water accumulation behind the bridge so-called “Backwater”. The simulation model has been run for two cases with the bridge and without the bridge to

investigate the effect of the bridge on the water level in the river. These simulations carried on with the presence of the levees and without them.

1) In the Presence of Levees

The levees have been applied on both sides of the river. The simulation has been run for both cases of “with bridge” and “without bridge” to assess the effect of the bridge on the backwater. The same model has been run with a 3-times higher flow rate to assess the effect of watershed size. As shown in figure 28 in the case of a 100-year flow rate, there are 1 ft of backwater behind the bridge and the effect lasts for about 3000ft behind the bridge and it will fade out eventually. In the case of 3-times higher flow, there are 8 ft of backwater behind the bridge and the effect is notable to the end of the domain.

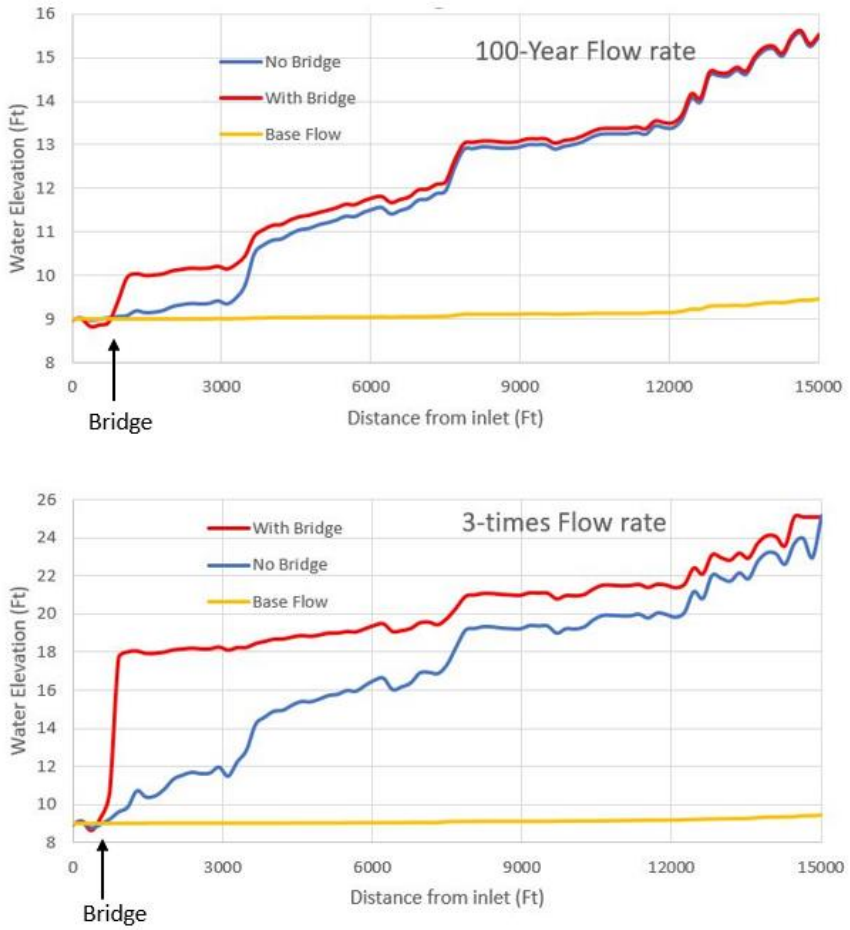

Figure 5.13 Backwater behind the bridge in the presence of levees for two cases of a 100-year flood and 3-times higher flow rate.

2) **Without Levees**

The levees have been deleted from the model and the effect of the bridge has been assessed on the backwater in the open domain for both cases of 9000 CFS and 27000 CFS. As It is shown in Figure 5.14, when there are no levees on the sides of the river, the effect of the presence of bridge is negligible and wide domain of marsh areas decrease the water elevation.

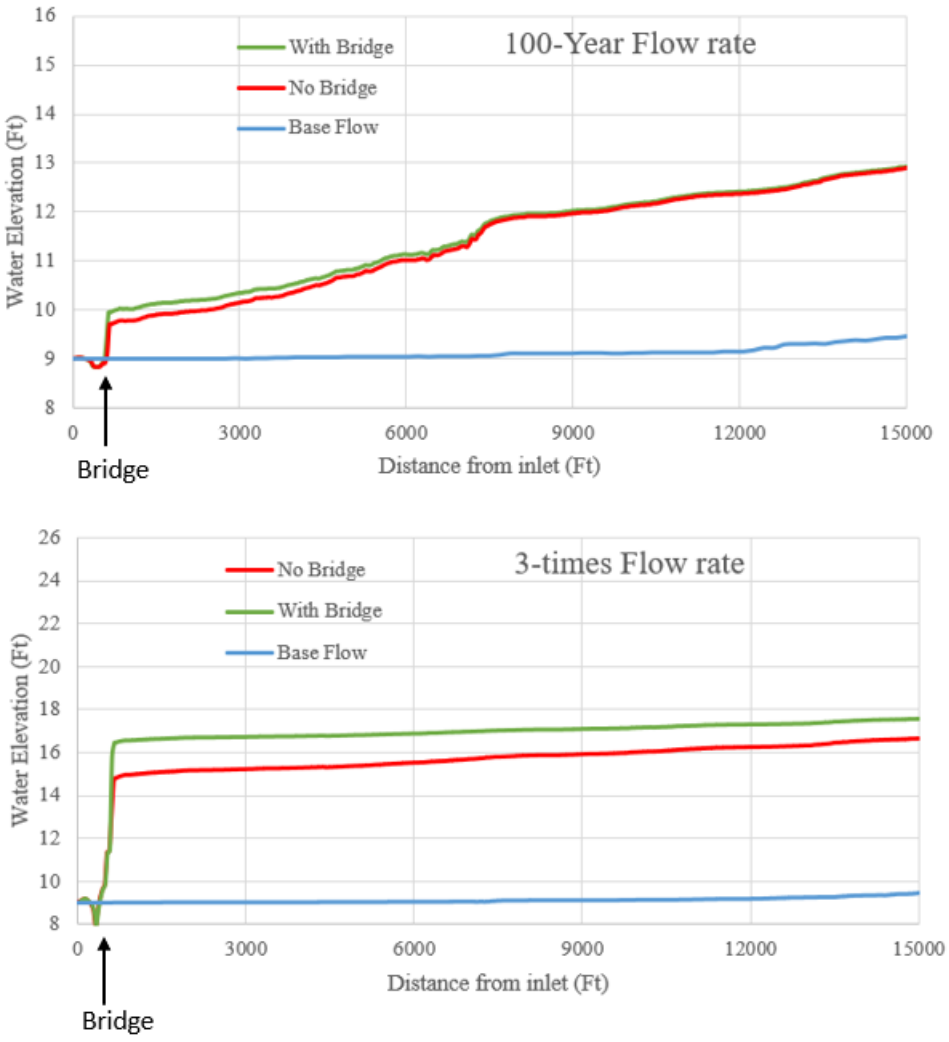

Figure 5.14 Backwater behind the bridge in case of no levees for two cases of a 100-year flood and 3-times higher flow rate.

To investigate the effect of the value of flow rate on the water level rise in the river, seven different historical storms have been chosen and applied over the study domain. Each precipitation value has been used as the input of the SWMM software and the corresponding outflow of them has been transferred into HEC-RAS. Table 5.1 shows the storms, precipitation rate and the corresponding flow rate in the river. Figure 30 shows the water level along the river for seven different storms, outputted from HEC-RAS.

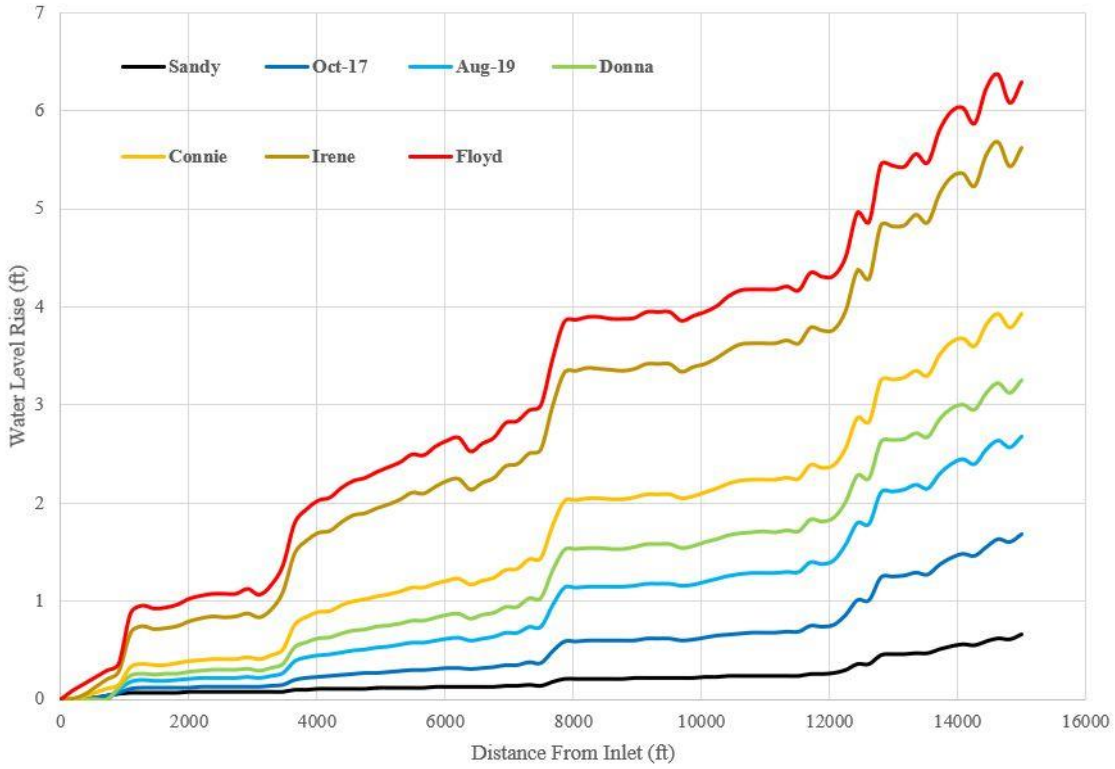

Figure 05.15 Water level rise along the river for different Historical storms.

Table 5.1 Historical Storms and their Corresponding Precipitation and River Outflow

Storm	Precipitation (in)	Outflow of the river (CFS)
Hurricane Sandy	1.2	160
10/30/2017	3.64	1250
08/08/2019	5.18	2400
Hurricane Donna	6.07	3100
Hurricane Connie	7.26	4000
Hurricane Irene	8.58	6500
Hurricane Floyd	10.3	7600

5.3 CHAMP

Figure 5.16 shows the result of WHAFIS for the extracted profile. The water propagates about 13000 ft into land for the defined storm. The MLLW and Hurricane Sandy storm surge is shown and compared in the figure by blue color. The highest wave crest is about 9 ft at the shoreline, and it keeps decreasing as the land elevation (water depth) decreases. (The CHAMP software only gives us the wave elevation from the start of the shoreline, and we don't have data about the wave elevation in the sea part, that's why the red line starts from x=0 ft). Since the topography of the area is very flat, the whole of the marsh area which is about 11500 ft is getting flooded and there are waves with crest of higher than 3 ft, so these lands are considered as a VE flood zone. After the marsh area, the topography land elevation starts to increase with steeper slope (3% slope). The urban area closer to the marsh area still doesn't have a proper elevation and they are getting flooded and are vulnerable to the strong waves. The first 1300 ft of the urban areas are in the VE flood zone, the next 500 ft would be in the AE flood zone and the rest of the area is safe. Figure 5.17 shows the effect of marsh areas by comparing the wave heights in the presence of vegetation and without them. The results show that the wave crest elevation has decreased up to 30% in wetland areas, but the wave height is almost the same in the residential areas at the end of the domain, since the shallower water depth and the wave breaking is the main reason for decreasing the wave height, not the vegetation.

There is another concept defined by FEMA which is the Limit of Moderate Wave Action (LiMWA). LiMWA is a line which is the inland limit of the area expected to receive 1.5 foot or greater breaking waves during the 1-percent-annual-chance flood event and the structures that are constructed without considering coastal hazards are getting huge damage

during these 100-year hurricanes. Figure 5.18 shows the LiMWA line for the urban areas next to Cheese-quake State Park. As you can see in Figure 5.18, there is a big part of the urban area which is vulnerable to flooding and wave action.

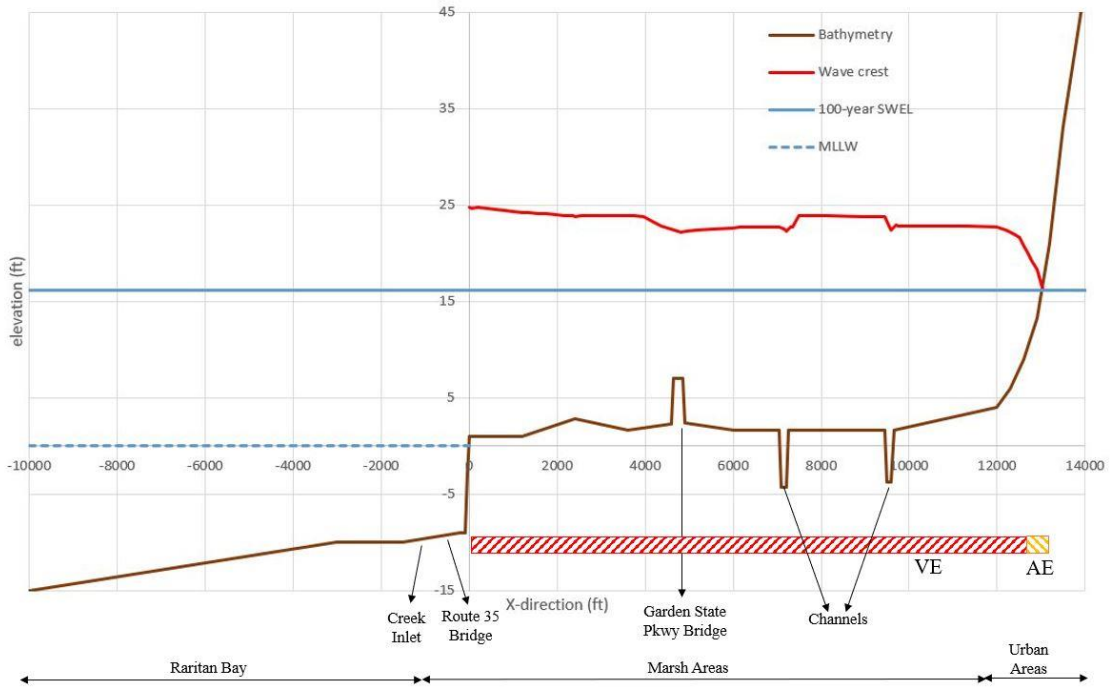

Figure 0.16 Results of the WHAFIS model for the chosen profile. The MLLW and 100-year SWEL can be compared in the figure. The elevation of the wave is shown by the red line and flooding zones are at the bottom of the figure.

Figure 5.17 Wave crest elevation in the presence of vegetation and without them.

Figure 5.18 LiMWA line for the urban area next to the Cheesequake Creek marsh area. The right side of the red line is vulnerable to the flooding and wave action of 1.5 ft.

Finally, the flooded areas have been calculated based on the Run-up module. In this case, the deep-water wave height is $H_0 = 10m$ and using Equation 3.35 the wavelength will calculate as $L_0 = 263m$. Using these values, the run-up elevation can be calculated from the FEMA formula (Equation 3.37). Figure 5.19 shows the results from the simulation which has good agreement with calculated vertical run-up from the FEMA analytical formula.

$$R_{u2\%} = 0.6\frac{\tan\alpha}{\sqrt{H_0/L_0}}H_0 = 0.6\frac{0.02}{\sqrt{10/250}}10 = 0.6m \tag{5.1}$$

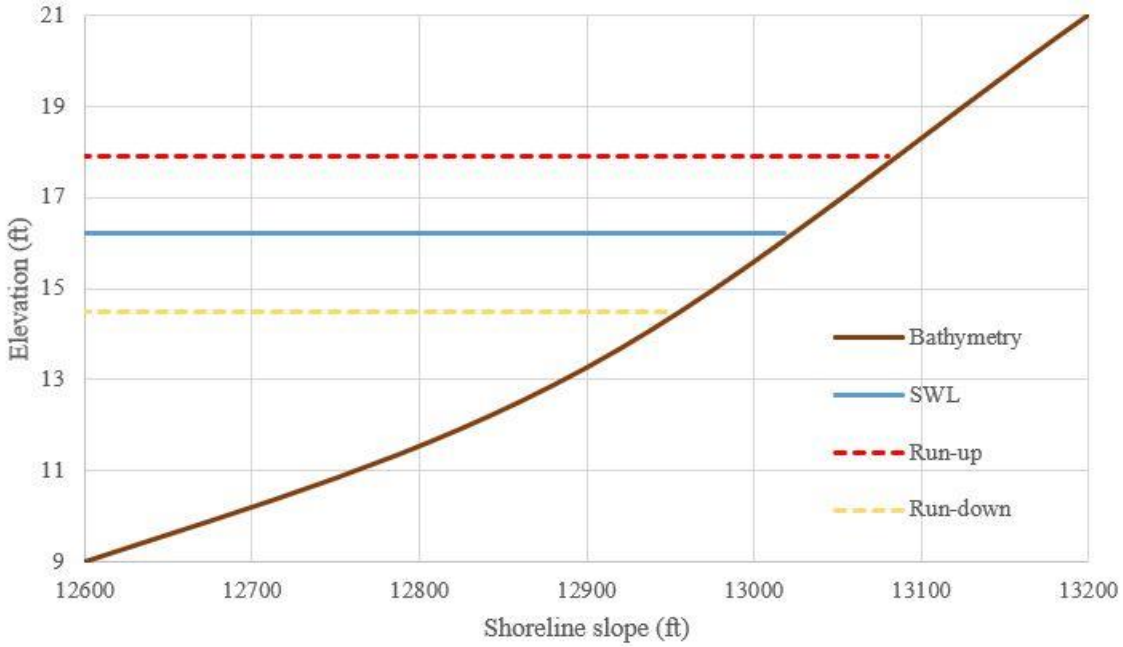

Figure 5.19 Run-up range for the urban areas at the end of Cheesequake Creek.

5.4 MIKE-21

5.4.1 Flow in the River

In the first part of modeling the water level in the ocean and river has been set to zero MSL and a steady flow rate of 7000 CFS (200 m3/s) has entered the domain from the west boundary (upstream of the river). As shown in Figure 5.20 the water fills up the river and overflows into the wetland areas. As expected, the water velocity is much higher in the main channel compare to the velocity of the water in the surrounding wetlands.

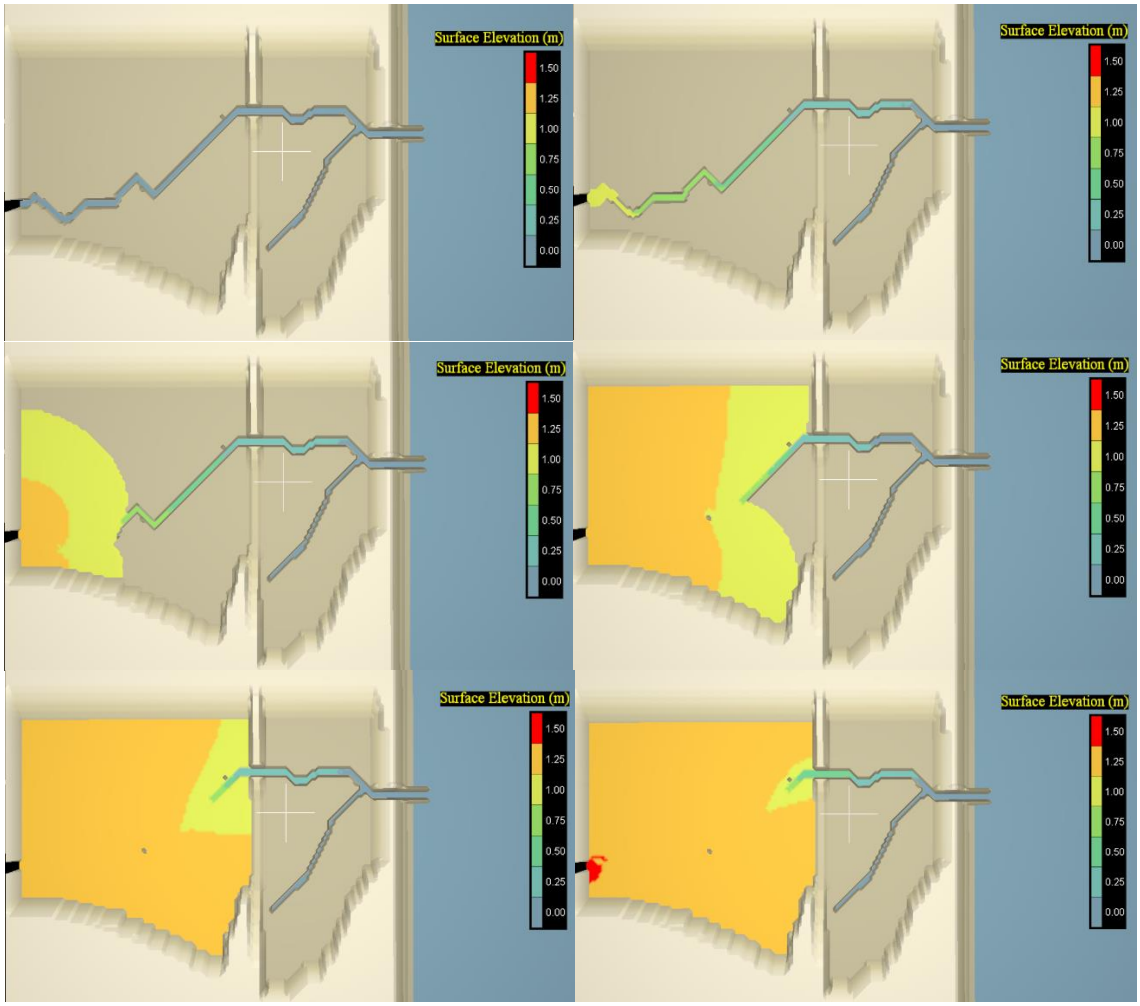

Figure 05.20. The water level in six different stages of the river inflow

In the second simulation, the levees have been modeled on both sides of the river to prevent the overflowing. The water level has been recorded along the river and results have been compared with the results of the HEC-RAS. Figure 5.21 shows the water level in both scenarios of the presence of levees and without them in MIKE-21 software and HEC-RAS. Since the water level in the ocean in zero MSL, all the graphs will tend to be zero at the inlet and as it got farther from the inlet, water level increases. There is less than 1 ft water level difference between the HEC-RAS model and MIKE-21 in most parts of the river.

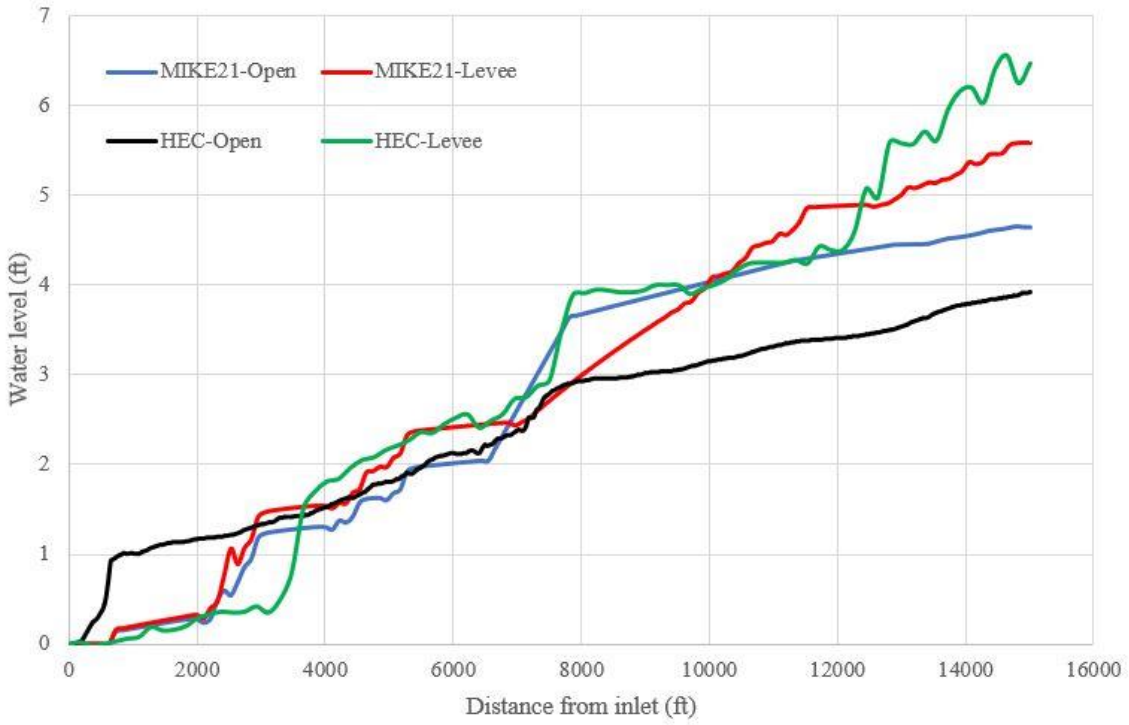

Figure 5.21 Water level along the river for both cases of with levee and without it from the simulations of MIKE-21 and HEC-RAS.

5.4.2 Ocean Storm Surge

The modeling of the ocean storms has been conducted in different stages:

1) Daily tide

2) Hurricane Sandy water level

3) Wave penetration

4) River flow rate for different storm surges

The daily tide of the Raritan Bay is about 2 m. The model has been run for 24 hr and the results show that the water level in the river is almost the same as the water level in the ocean. Since the river size and the marsh areas around it are small, the domain will fill very fast with 30 minutes delay compare to the ocean.

The water level rise of Hurricane Sandy for the location of Sandy Hook (which is the closest station to our domain) has been extracted from the NOAA website and applied to the east boundary of the domain. The water level has been recorded inside and outside of the bay and the results have been compared in figure 5.22 There is a small delay for the time of the peaks and a small difference in the value of them. When the main storm hits the shoreline, everywhere getting flooded and the peaks are matches inside and outside of the bay.

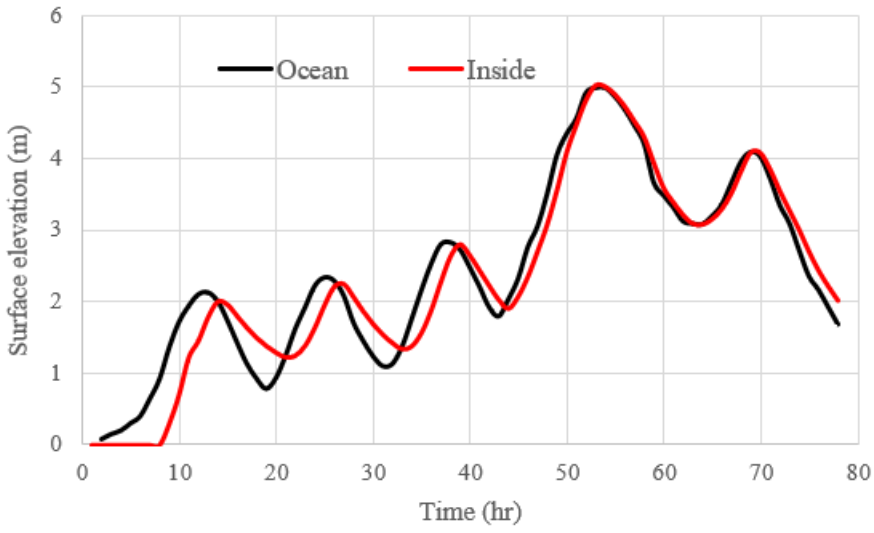

Figure 5.22 The water level inside and outside of the bay during Hurricane Sandy.

The peak of the storm (5 m storm surge) has been considered as the critical condition and the significant wave heights of 8 m has been applied over this storm surge to calculate the penetrated waves into the bay. Figure 5.23 shows the surface elevation for the offshore wave, the wave height near the shoreline and the wave heights inside the bay. As shown below, the offshore wave heights of 8 m have been decreased to 2.5 m near the shoreline and penetrated wave inside the bay is less than 0.5 m which can be neglected compared to the offshore wave heights. Figure 5.24 shows the water level in a random time-step during the wave penetration simulation. The color palette shows the negligible penetrated wave into the Cheesequake park.

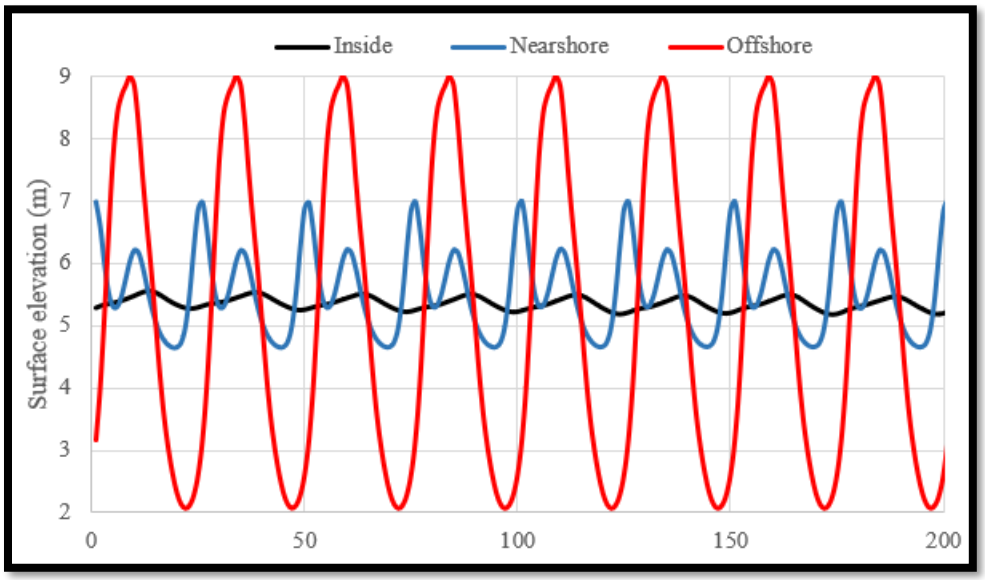

Figure 5.23 wave height at THREE different locations of offshore, nearshore and inside the bay during the peak of Hurricane Sandy.

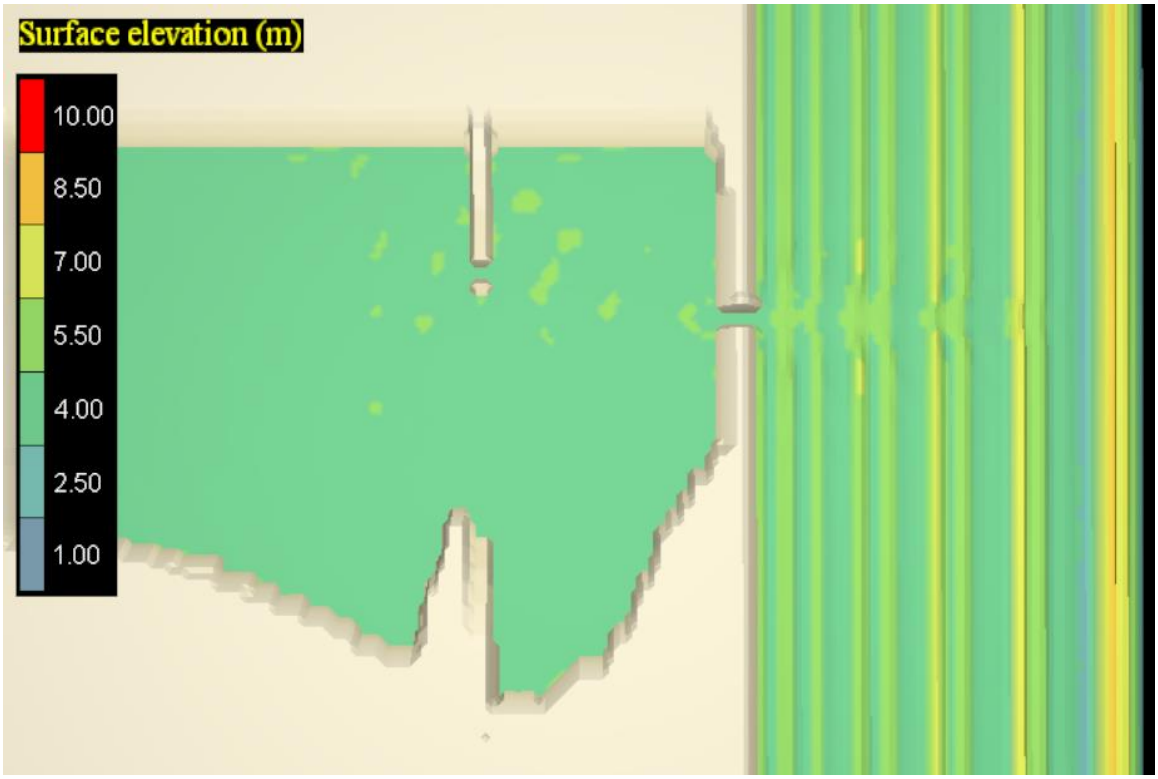

Figure 5.24 Negligible wave penetration into the study domain.

In the final stage, the flow rate of the river has been applied to the different storm surge to assess the effect of the combination of precipitation and offshore storm surge. Figure 5.25 shows the surface elevation map for the river flow rate of 200 m^3/s applied over the mean sea level. As shown the highest water level reaches 1.5 m in upstream and the water level decreases to zero to match with the water level in the ocean.

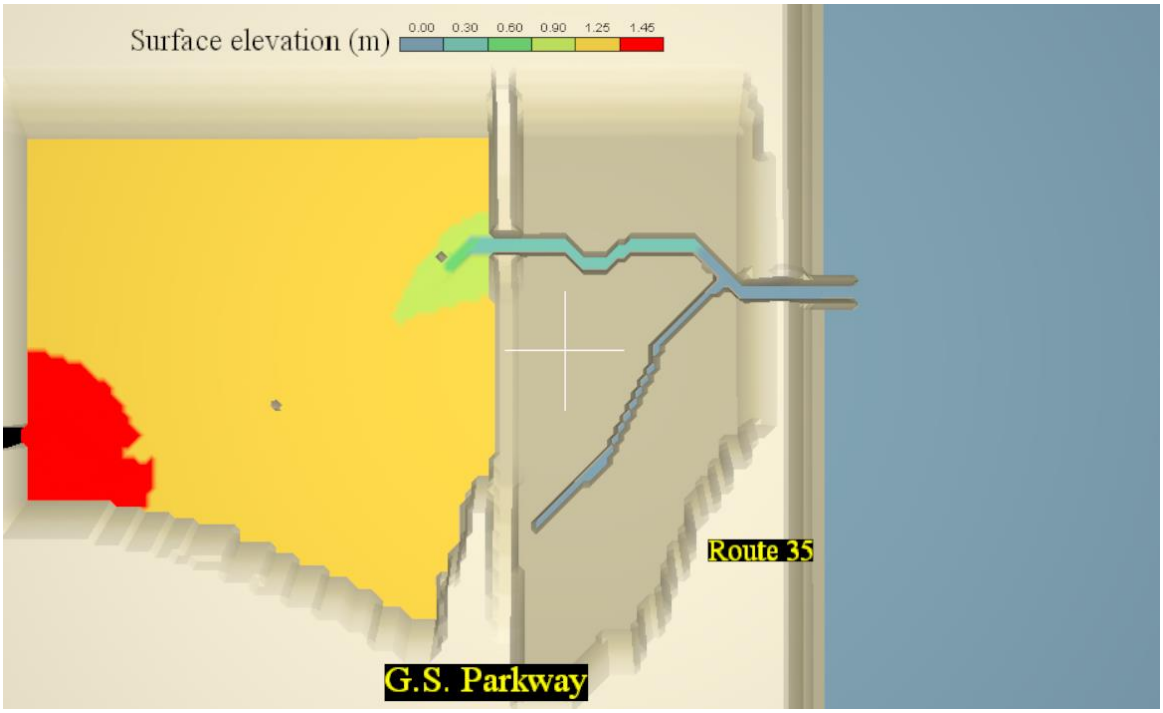

Figure 5.25 The surface elevation map for the flow rate of 200 applied over the mean sea level.

The ocean storm surge has been changed from -1m (low tide) to 5 m (Hurricane Sandy) and a flow rate of 200 m3/s has been applied to the different storm surge. The water level rise based on these different conditions has been calculated in the river. Figure 5.26 shows the water level in the study domain during the 100-years return period rainfall co-occurred with a storm surge of 2 m (left panel) and a storm surge of 4 m (right panel). Figure 5.27 shows the diagram of the water level rise during the 100 years return period rainfall the river co-occurred with the different storm surges. As shown in the figure, the effect of the rainfall decreases as the storm surge increases. It means there is the highest water level rise caused by the rainfall during the low tides. Around the storm surge of 4 m, the water level rise caused by the rainfall is almost zero and totally negligible.

It is important to mention that the water level on the right boundary is set to a certain elevation, assuming that the water level rise in the bay which caused by the rainfall cannot affect the water level in the ocean. It cannot be neglected that this assumption can affect

the results. Based on the river hydraulic theories, water level rise in the river is governing by the slope of energy level line. Since the outlet boundary of the system has been fixed to a certain elevation, therefore the water level in the domain is bounded by a certain value.

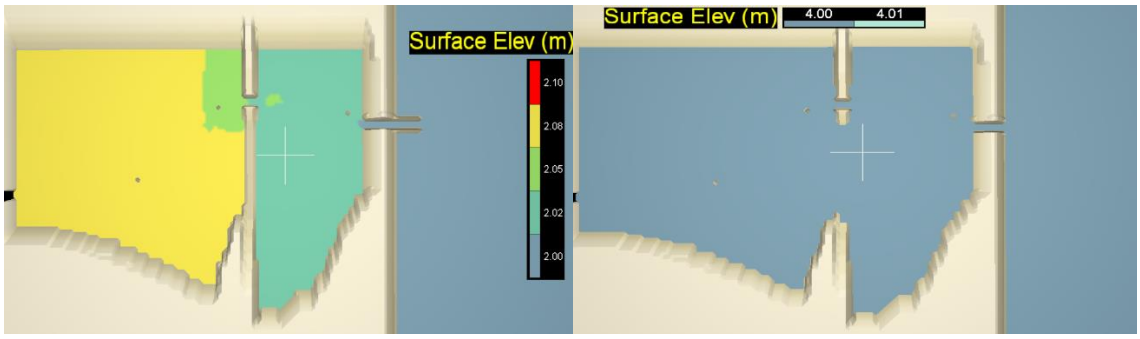

Figure 5.26 Surface elevation for the compound flooding of 2 m storm surge (left panel) and a surge of 4m (right panel)

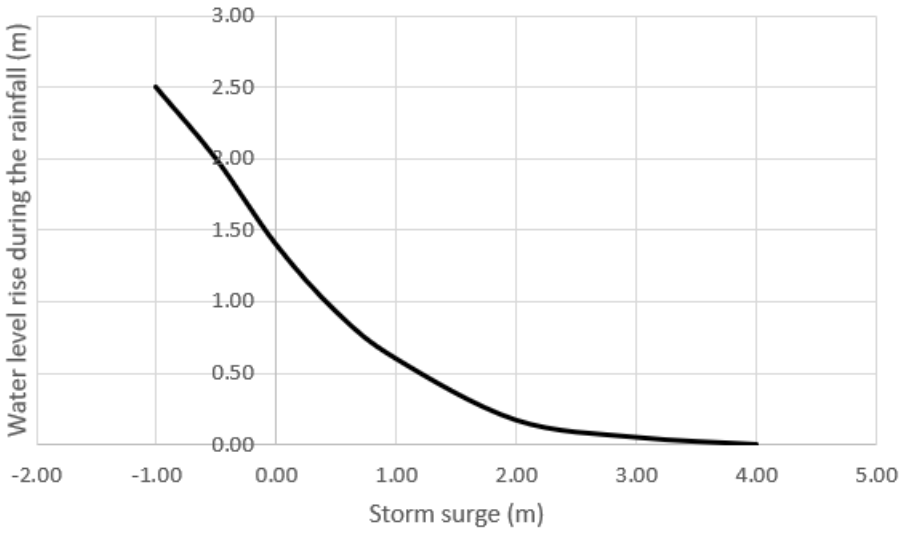

Figure 5.27 Water level rise during the 100 year return period rainfall event in the function of different storm surges.

SUMMARY AND CONCLUSION

- Chapter 1 explained the main issue of flooding in coastal areas. The vulnerability of low land coastal areas against inland and offshore event has evaluated and some historical data have presented to demonstrate the magnitude of the disaster.
- Chapter 2 addressed the previous studies in this field. It explained how the offshore hurricane and heavy precipitation can damage the coastal areas and what happens when these two events happen at the same time.
- The main propose of Chapter 3 was to introduce the software and tool which has been exploited to solve the problem. The Governing equations of HEC.RAS, SWMM, CHAMP, and MIKE21 have presented
- Chapter 4 addressed the methods of current research. It explains how we utilized the different software, what approaches have chosen for the simulations and based on that approach which practical constants have been applied to find the realistic results.
- Chapter 5 is presenting the results of the simulations. The summary of the results can be presented in the form of bullet points below:
    - Urban areas show a faster response to the heavy precipitation compared to the wetlands. This faster response will result in a higher flow rate which increases the chance of flooding.
    - Changing the shape of the cross-section and width of the river can cause a huge difference in flow regime, water velocity, and water level.

- Results show that for the steady-state analysis for the small river such as Cheesequake Creek, the water level rise in the upstream of the creek is more severe than the downstream.
- The presence of a bridge in cross-section a river can cause the backwater phenomena which can drastically increase the water level in different locations of the river.
- The effect of the wetland areas has been investigated. Results show that these wetlands have a high effect on mitigating the flooding level in the study domain.
- Applying levees on both sides of the Creek will terminate the effect of the wetland areas and can cause unpredicted level of flooding.
- The results of CHAMP software show the water level rise in different location of the study domain caused by the offshore storm and the highest recorded water level in the domain is about 22 ft.
- Then the effect of wetland areas has been investigated on the flood level mitigation from the offshore event. The maximum flood level decrease of 30% has been recorded in the study domain.
- The run-up elevation has been calculated by CHAMP software and it shows 3 ft run-up elevation which directly affects the urban areas.
- MIKE-21 simulation has been conducted to model the compound flooding in the study domain.

- The result from the modeling of waves in MIKE-21 shows the very small wave penetration into the study domain based on the size of the bay and inlet.
- The water level rise of the domain has been recorded during compound flooding. Results demonstrated that the effect of compound flooding has a strong relationship with the base water level.
- As the magnitude of the offshore storm increases, the effect of flooding caused by the precipitation decreases. For instance, The water level rise form the precipitation is 2.5 m during the low tide, it decreases as offshore storms get stronger and it eventually fades out after the water level rise based on the offshore event is about 4m.

FUTURE STUDIES

There are a lot more to be done in the field of coastal flooding such as:

- Investigate different types of statistical methods to have a better understanding of the probability of compound flooding.
- The inlet of the bays is exposed to the both direction water flows, which can happen through precipitation, offshore storm, and daily tides. This complicated flow regime, especially in the presence of a bridge on the inlet needs a lot of attention.
- In this study, the effect of small bay inlet and wetland areas has been investigated in mitigating the flood magnitude in the coastal areas. Different types of natural phenomena can help us to protect our coastal areas which can be exploited in future studies.
- By advancing the CFD methods, this study can be conducted by future software which gives us more accurate results since they are faster, and they can perform with much smaller mesh size.

REFERENCES

Ahrens P, 1981. Irregular Wave Runup on Smooth Slopes, COASTAL ENGINEERING RESEARCH CENTER, Fort Belvoir, VA.

Bellomo D and Sparks J, 1999. Coastal flood hazards and the national flood insurance program, Journal of Coastal Research: 21-26.

Burcharth H and Hughes S, 2002. Fundamentals of Design, Coastal Engineering Manual, Part VI - Chapter VI, US Army Corps of Engineers.

Kemp C and Horton B, 2013. Contribution of relative sea-level rise to historical hurricane flooding in New York City.

DiGiano F, Adrian D, Mangarella P, 1977. Short Course Proceedings: Applications of Stormwater Management Models, Environmental Protection Agency, Office of Research and Development.

Douglas I, 2018. The challenge of urban poverty for the use of green infrastructure on floodplains and wetlands to reduce flood impacts in intertropical Africa, Landscape and Urban Planning, 180: 262-72.

EurOtop, 2007. Wave overtopping of sea defences and related structures: assessment manual.

FEMA, 2015. Guidance for Flood Risk Analysis and Mapping, Overland Wave Propagation.

Hecker GE, 1996. Hydrology Handbook: ASCE Manuals and Reports on Engineering Practice No. 28, American Society of Civil Engineers, New York.

Hendry A, Haigh I, Nicholls R, Winter H, Neal R, Wahl T, Joly-Laugel A, Darby S, 2019. 'Assessing the characteristics and drivers of compound flooding events around the UK coast', Hydrology and Earth System Sciences, 23: 3117-39.

Hsu T, Liang S, Young B, Ou S, 2012. Nonlinear run-ups of regular waves on sloping structures, *Nat.* Hazards Earth Syst. Sci., 12: 3811-20.

Hughes A, St. Denis L, Leysia P, Anderson K, 2014. Online public communications by police and fire services during the 2012 Hurricane Sandy. SIGCHI Conference on Human Factors in Computing Systems, 1505-14. Toronto, Ontario, Canada: ACM.

Hughes A, 2004. Estimation of wave run-up on smooth, impermeable slopes using the wave momentum flux parameter, Coastal Engineering, 51: 1085-104.

Hunt I,, 1959. 'Design of sea-walls and breakwaters', Transactions of the American Society of Civil Engineers, 126: 542-70.

Jean-Baptiste N, Kabisch S, Kuhlicke Ch, 2013. Urban vulnerability assessment in flood-prone areas in West and East Africa. in, Urban environment (Springer).

Kalyanapu A, Burian S, McPherson T, 2010. Effect of land use-based surface roughness on hydrologic model output, Journal of Spatial Hydrology, 9.

Kendall M, 1938. 'A new measure of rank correlation', Biometrika, 30: 81-93.

Kumbier K, Carvalho R,Vafeidis A, Woodroffe C, 2018. Investigating compound flooding in an estuary using hydrodynamic modelling: a case study from the Shoalhaven River, Australia.

Lin N, Kopp R, Horton B, Donnelly J, 2016. Hurricane Sandy's flood frequency increasing from year 1800 to 2100, Proceedings of the National Academy of Sciences, 113: 12071-12075.

Losada M, Giménez Curto L, 1980. Mound breakwaters under wave attack, Department of Oceanographical and Ports Engineering.

Marsooli R, Orton P, Mellor G, 2017. Modeling wave attenuation by salt marshes in Jamaica Bay, New York, using a new rapid wave model, Journal of Geophysical Research: Oceans, 122: 5689-707.

Mase H, 1989. Random wave runup height on gentle slope, Journal of Waterway, Port, Coastal, and Ocean Engineering, 115: 649-61.

Ng W, Mendelsohn R, 2005. 'The impact of sea level rise on Singapore', Environment and Development Economics, 10: 201-15.

NOAA, National Oceanic and Atmospheric Administration, 2012b. NOAA Tides and Currents. National Oceanic and Atmospheric Administration, Washington, DC. http://tidesandcurrents.noaa.gov/. 2013. National coastal population report: population trends from 1970 to 2020.

Noori N, Kalin L, Sen S, Srivastava P, Lebleu Ch, 2016. Identifying areas sensitive to land use/land cover change for downstream flooding in a coastal Alabama watershed, Regional Environmental Change, 16: 1833-45.

Orton P, Talke S, Jay D, Yin L, Blumberg A, Georgas N, Zhao H, Roberts H, MacManus K, 2015. Channel shallowing as mitigation of coastal flooding, journal of marine science and engineering, 3: 654-73.

Pardue J H, Moe D, McInnis L J, Thibodeaux K T, Valsaraj E, Maciasz I, van Heerden N, Korevec and Q Z Yuan, 2005. 'Chemical and microbiological parameters in new orleans floodwater following hurricane katrina', Environmental Science & Technology, 39: 8591-99.

Rodi W, 1984. 'Turbulence models and their applications in hydraulics-a state-of-the-art review', *IAHR* monograph.

Sado-Inamura Y and Fukushi K, 2019. 'Empirical analysis of flood risk perception using historical data in Tokyo', Land Use Policy, 82: 13-29.

Shepard C, Crain C, Beck M, 2011. The protective role of coastal marshes: A Systematic Review and Meta-analysis, PLOS ONE, 6: e27374.

Smallegan St, Irish J, Van Dongeren A, Den Bieman J, 2016. Morphological response of a sandy barrier island with a buried seawall during Hurricane Sandy, Coastal Engineering, 110: 102-10.

SPM, 1984. *USA. Army.* Coastal Engineering Research Center, Shore protection manual (Department of the Army, Waterways Experiment Station, Corps of Engineers).

Svensson C and Jones D, 2006. Joint Probability: Dependence between extreme sea surge, river flow and precipitation: A study in South and West Britain, Dep Environmental Food Rural Affairs, London.

Wang H, Loftis J, Liu Zh, Forrest D, Zhang J, 2014. The storm surge and sub-grid inundation modeling in New York City during Hurricane Sandy, Journal of Marine Science and Engineering, 2: 226-46.

Wang Sh and Christensen B, 1987. Friction in hurricane-induced surges. Coastal Engineering.

Ward Ph, Couasnon A, Eilander D, Haigh I, Hendry A, Muis S, Veldkamp T, Winsemius H, Wahl T, 2018. Dependence between high sea-level and high river discharge increases flood hazard in global deltas and estuaries, Environmental Research Letters, 13: 084012.

Wassing F, 1957. Model investigation on wave run-up carried out in the Netherlands during the past twenty years, Coastal Engineering Proceedings, 1: 42.

Wei Zh, Dalrymple R, Hérault A, Bilotta G, Rustico E, Yeh H, 2015. SPH modeling of dynamic impact of tsunami bore on bridge piers, Coastal Engineering, 104: 26-42.

Woodruff J, Irish J, Camargo S, 2013. Coastal flooding by tropical cyclones and sea-level rise, Nature, 504: 44.

Zheng F, Westra S, Leonard M, Sisson S, 2014. Modeling dependence between extreme rainfall and storm surge to estimate coastal flooding risk, Water Resources Research, 50: 2050-71.